An Analysis of the Nuclear Characteristics of a Molten Salt Microreactor

A Thesis
Presented in Partial Fulfillment of the Requirements for the
Degree of Master of Science
with a
Major in Nuclear Engineering
in the
College of Graduate Studies
University of Idaho
by
John Peterson

Major Professor: R.A. Borrelli, Ph.D.
Committee Members: Leslie Kerby, Ph.D.; Richard Christensen, Ph.D.
Department Administrator: Richard Christensen, Ph.D.

August 2019

Authorization to Submit Thesis

This thesis of John Peterson, submitted for the degree of Master of Science with a Major in Nuclear Engineering and titled "An Analysis of the Nuclear Characteristics of a Molten Salt Microreactor," has been reviewed in final form. Permission, as indicated by the signatures and dates below is now granted to submit final copies for the College of Graduate Studies for approval.

Major Professor:	R.A. Borrelli, Ph.D.	Date
Committee Members:	Leslie Kerby, Ph.D.	Date
	Richard Christensen, Ph.D.	Date
Department Administrator:	Richard Christensen, Ph.D.	Date

Abstract

This work evaluates several neutronics-related performance characteristics of a proposed molten salt micro-reactor. The Molten Salt Nuclear Battery is a liquid fuel molten salt system designed to be entirely self-contained, circulate the fuel and salt through natural convection, and provide 10 MW of thermal power for up to 10 years of continuous operation. Areas of investigation include candidate neutron reflecting and absorbing materials, control rod design and optimization, criticality control, neutron flux profile characterization, reactor operation and fuel burnup, fission product production, and radioactive dose in close proximity following shutdown. The primary means of investigation was simulation with the MCNP and ORIGEN codes. The analysis shows that the proposed design can meet the desired operational parameters and that control of the reactor is achievable with the optimized control rods, while also quantifying other essential nuclear characteristics. Assumptions and simplifications used in the simulations and the avenues of further research are discussed.

Acknowledgments

Writing a thesis was an entirely new challenge that I was not wholly prepared for; up until this point, I had been given a problem and pointed in the correct direction to find the solution. In this work, I did not know whether there was even a solution until I had found it. The support given by Dr. Bob Borrelli was essential for me to complete this project. His dedication to his students and their success is second to none, and being able to rely on his technical expertise was invaluable when I did not know how to even begin to approach a problem.

The guidance of Dr. Richard Christensen was vital in bringing this work from start to finish. Rather than giving direct advice or instructions, he simply asked the right questions. His active involvement in this research led to to exciting discoveries and overcoming a number of technical challenges.

Dedication

This thesis is dedicated to my mother and father, for cultivating my fascination with the natural world and for their endless love and support. Thanks, Mom and Dad.

Table of Contents

List of Tables

List of Figures

List of Acronyms

BeO	Beryllium Oxide
CFD	Computational Fluid Dynamics
FLiBe	$LiF-BeF_2$
FLiNaK	$LiF-NaF-KF$
LWR	Light Water Reactor
JEFF	Joint Evaluated Fission and Fusion
MCNP	Monte Carlo N-Particle
MSNB	Molten Salt Nuclear Battery
MSR	Molten Salt Reactor
MSRE	Molten Salt Reactor Experiment
NPP	Nuclear Power Plant
ORIGEN	Oak Ridge Isotope Generation
UF_4	Uranium Tetrafluoride

Chapter 1: Introduction

There is a growing need for reliable and compact sources of small-scale electrical power. Locations that are not connected to a wider electrical grid such as islands, off-grid industrial sites, and fixed Department of Defense installations often require frequent shipments of fossil fuels to meet baseload energy demands [1]. Interruption of these shipments can lead to a necessary reduction in electricity consumption or even a complete loss of electrical power, which may be unplanned and cause significant disruptions. Nuclear microreactors are able to fill this need by supplying long-term thermal and electrical power without a reliance on frequent refueling shipments or maintenance. This work describes an investigation of the nuclear characteristics of a proposed molten salt microreactor design to conducted determine its applicability.

1.1 Background

To meet this need, a number of companies are developing nuclear microreactor designs. For the purposes of this work, a microreactor is defined as a compact, self-contained nuclear reactor that produces less than 50 MW thermal power. Microreactors are expected to produce a small amount of electrical power for a long period of time without requiring refueling or extensive maintenance, and are intended to be assembled, shipped, and installed as a single unit. Westinghouse, NuScale, and General Atomics are only a few of the companies that are currently advancing microreactor designs [1]. Of the proposed designs, most utilize solid fuel elements similar to those used in commercial nuclear power plants, along with the associated cooling, electrical conversion, and safety systems. Nuclear reactors relying on these designs are well understood and have years of operational experience, which supports design, licensing, and regulatory efforts. However, these microreactors have many of the same limitations of the commercial reactors on which they are based, particularly the reliance on forced circulation of the reactor coolant and the lack of passive safety features. Both disadvantages can be overcome by utilizing a Molten Salt Reactor (MSR) design.

The original MSR concept was developed at Oak Ridge National Laboratory in the 1950s [2]. The Molten Salt Reactor Experiment (MSRE) was completed in 1965 and operated until 1969, demonstrating that such a design was practical and could be operated safely, reliably, and without difficulty. The MSRE utilized a Uranium Tetrafluoride (UF_4) fuel dissolved in a $LiF-BeF_2$ (FLiBe) molten salt that operated as both a carrier for the fuel and a coolant for the system [2]. The use of a molten salt and liquid fuel allows a nuclear reactor to operate indefinitely due to an inherent resistance to radiation damage and at high temperatures and low fluid pressures, which lead to efficient energy production and inherent safety. These features are beneficial in nuclear power plants ranging in size from large-scale commercial facilities to the small, standalone microreactor units proposed. Since the completion of the MSRE project, much of the focus in the deployment of nuclear power has been with Light Water Reactors (LWRs). However, interest in MSRs has been revived with the development of Generation IV nuclear reactors because of the unique advantages afforded by the design. MSR designs are particularly well-suited for the development of microreactors because of their simplicity, efficiency, and passive safety.

1.2 Scope

This work involves characterizing the nuclear characteristics of a proposed molten salt microreactor design, referred to as the Molten Salt Nuclear Battery (MSNB). The MSNB uses UF_4 dissolved in FLiBe as the fissile fuel and primary reactor coolant, which is passively circulated through the system by natural convection. The design is further simplified by the use of sodium heat pipes to remove heat from the system, which is transferred to a secondary helium coolant that is used to produce electricity. The system is intended to operate for up to 10 years at 10 MW thermal power without needing to be refueled. To achieve this, the uranium is enriched to 20% ^{235}U and the UF_4 constitutes 7% of the mixture by weight. Taken together, these properties describe a system that requires little operator input, is passively safe, and provides reliable baseload power for an extended period of time. The MSNB design is advantageous as compared to other proposed microreactor designs primarily because of the safety and reliability afforded by the liquid fuel and molten salt system.

1.3 Outline

This report will discuss the theory of MSR operation and the properties and advantages of molten salts and liquid fuels. The computational tools available for the analysis of nuclear systems, specifically the Monte Carlo N-Particle (MCNP) and Oak Ridge Isotope Generation (ORIGEN) codes, will be examined. The underlying mathematical and statistical basis of the methods utilized by the computational tools will be discussed, as well as the means by which the accuracy of the results can be improved. The discussion will then move to the selection of materials for use in the construction of the MSNB, calculation of physical parameters of the FLiBe-UF_4 mixture to be used in computer simulations, and the design and optimization of the control rods used in maintaining the fission chain reaction. Characterization of the various profiles of neutron flux in the reactor core will then be investigated. Next, operation of the MSNB will be simulated, with the results used to inform investigations of the production of fission products and the radioactive dose expected in proximity to the reactor following operation. Finally, the assumptions used in the study and the limitations of the methods used will be discussed in the context of future research to be conducted.

Chapter 2: Molten Salt Reactor Theory

2.1 Molten Salt Reactor Operation

An MSR is a type of nuclear fission reactor that utilizes a molten salt mixture as the primary reactor coolant or as a carrier for a liquid nuclear fuel. In the first case, the molten salt serves as a low pressure, high temperature coolant to a critical arrangement of solid fissile fuel installed in the reactor core. In the second case, the molten salt acts as both a coolant and carrier for a liquid fissile fuel circulating throughout the reactor and critical core region. For the purposes of this work, only theory relating to this second case will be discussed, as the MSNB is of this type.

Liquid fuel MSRs operate by circulating a fuel-carrying molten salt throughout the entirety of the primary loop of the reactor. The composition of the mixture and physical geometry of the system ensure that it is inherently subcritical everywhere but in the core of the reactor, wherein criticality is achieved through the use of a geometrically favorable containment volume as well as neutron moderators, reflectors, or both. As the rate of nuclear fissions in the fuel rapidly increases to a steady state in the core region, the energy released by these events is captured by the molten salt as heat. The heated salt exits the critical region and passes through a heat exchanger, where it transfers the energy to a secondary loop before returning to the core. In some cases, the fluid in the secondary loop can pass through another heat exchanger to transfer the heat to a fluid in a tertiary loop. The addition of a tertiary loop allows for the heat produced in the reactor core to be ultimately transferred, by means of the intermediary fluid in the secondary loop, to a fluid that, in contrast to the molten salt utilized in the primary loop, has not been exposed to high levels of radiation and is typically less chemically volatile. The heated fluid in the final loop of the system, whether it is the secondary or tertiary, is used to drive the rotation of a turbine and generator to produce electricity. In large facilities, after the cooled molten salt in the primary loop exits the heat exchanger and before it reenters the core, some designs call for diversion to an on-site chemical plant where the chemical balance of the molten salt is maintained. In the chemical plant, physical and pyrochemical processes are employed to remove fission products and actinides from the salt while the fuel inventory is replenished through the addition of fissionable isotopes, after which the molten salt is returned to the primary loop. An MSR system with primary, secondary, and tertiary loops is visualized in Figure 2.1 [3].

Online control of the rate of nuclear fission in an MSR is achieved immediately through the use of neutron absorbing control rods and in the long term through the management of the molten salt chemistry in the on-site chemical plant. The control rods, typically actuated by inserting or removing them vertically within the core, contain enough excess negative reactivity to fully stop the nuclear fission reaction, if needed. In an accident scenario that in some way renders the control rods ineffective, MSR designs include a freeze plug located at a low point in the system. The freeze plug is designed such that at a certain temperature above the maximum operating temperature of the reactor, which the molten salt is expected to exceed in an accident scenario, the plug melts and quickly drains the liquid contents of the system into a series of emergency dump tanks. Because the molten salt carries the fuel and is removed into a subcritical configuration within the tanks, the nuclear reaction immediately stops. In

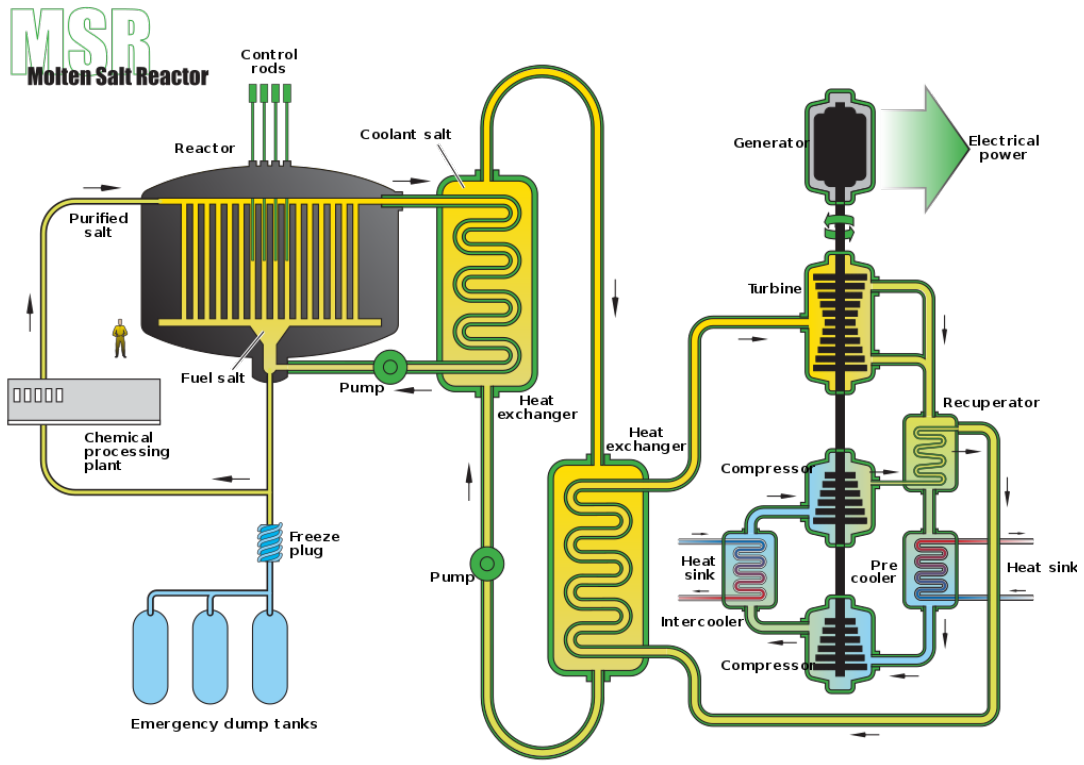

Figure 2.1: Diagram of a generic molten salt reactor

such an event, only the heat produced by decaying unstable isotopes already contained within the salt needs to be regulated.

2.1.1 Molten Salts

Salts are ionic chemical compounds produced by the neutralization reaction of an acid and base. Those which are solid at standard temperature and pressure but melt into a liquid phase at elevated temperatures are described as molten salts. These materials have been investigated for use as coolants in advanced nuclear reactor designs because of a number of advantageous qualities they possess over other proposed coolants while in the liquid phase, particularly their thermal and nuclear properties. The molten salts proposed for use in MSR designs are often fluoride salts, two of the most widely investigated of which are FLiBe and LiF–NaF–KF (FLiNaK) [4]. Both have advantageous thermal properties, but FLiBe is the focus of research as a primary reactor coolant due to its superior nuclear properties. In particular, the total neutron interaction cross section of FLiBe is lower than that of FLiNaK due to the large neutron capture cross section of potassium [5]. Utilization of a molten salt with a lower neutron cross section leaves a greater fraction of fission neutrons available to interact with the carried fissile fuel.

Two of the three elemental components of FLiBe, fluorine and beryllium, are naturally composed of only one stable isotope and have only extremely short-lived unstable isotopes. Because different isotopes of the same element can have drastically different nuclear properties, the comparatively small range of

isotopes in the elements that constitute the bulk of the molten salt allows for better predictions of the bulk nuclear properties of the material.

Alongside fluorine and beryllium, FLiBe also contains significant quantities of lithium, which at natural abundances is composed of several percent of the isotope ^{6}Li. ^{6}Li has a significant neutron absorption cross section in the thermal neutron energy range and can be detrimental to the neutron economy of the reactor. Thus, it is a requirement that the production of FLiBe for use in an MSR uses lithium with as pure ^{7}Li, the most significant isotopic constituent of natural lithium, as possible.

FLiBe has a viscosity similar to that of water and a density much lower than comparable liquid metals proposed for use in other advanced reactor designs [4], which allows for it to be more easily pumped through a system and makes it particularly suitable for natural circulation systems. The volumetric heat capacity of FLiBe is greater than that of pressurized water, helium, and sodium, the latter two of which are other proposed advanced reactor coolants [6]. Among molten salts of interest, FLiBe has the highest volumetric heat capacity and thermal conductivity, allowing it to take in large amounts of energy in the critical nuclear core and then effectively transfer that energy away to the secondary coolant [4].

One of the most significant disadvantages of FLiBe is its chemical volatility, especially at the high temperatures expected within an MSR. An ongoing area of research is the corrosion effects of high temperature FLiBe on materials typically used in the construction of nuclear reactors, such as stainless steel, zirconium alloys, and graphite.

While there is extensive data on the physical and nuclear properties of pure FLiBe, less is known about these properties for the mixture of FLiBe and UF_4. For example, the density of the mixture has not been measured. Although approximations can be made, such as averaging the densities by mass fraction of the constituents, the actual density of the mixture may be drastically different [7].

2.1.2 Liquid Fuel Systems

The molten salts proposed for use in a liquid fuel MSR typically form eutectic mixtures with the nuclear fuels. Eutectics are those mixtures that have a lower melting temperature than any of the individual components of the mixture. In the context of an MSR, this results in a mixture that is more easily melted and introduced into the system at the beginning of operation, and will remain as a liquid for a longer period of time if the nuclear fission chain reaction is slowed or stopped for any reason.

Some liquid fuel MSR designs have been developed to use the thorium fuel cycle, which uses fertile ^{232}Th that is transmuted to fissile ^{233}U, or fissile uranium isotopes directly as the nuclear fuel. Because thorium naturally contains only traces of fissile isotopes, such as ^{231}Th, pure thorium as a fuel is insufficient to begin the nuclear reaction, requiring the addition of fissile isotopes at reactor startup [2]. The most studied means of including the fissile or fertile fuels in the liquid fuel system is through the use of fluoride compounds, typically UF_4 and ThF4.

Liquid fuel MSRs systems are advantageous as compared to conventional LWRs, which are solid fuel element systems, for a number of reasons. Because they operate close to ambient pressures, the risk of a pressure-related explosion in an MSR during an accident scenario is low. At the same time, the relatively high temperatures produced in an MSR lend themselves to more efficient electricity production or coupling to high temperature industrial processes. Conventional LWRs operate with core outlet temperatures

around 300°C; MSR designs typically have outlet temperatures of 700°C or more [2]. Using the high temperature output of an MSR to directly supply an industrial process bypasses the thermal to electrical energy conversion process, which typically has efficiencies around 30-40%. In the context of hydrogen production through high temperature electrolysis processes, "with increasing temperature of operation, the electrical power input requirements decrease with balance of energy being provided by the heat...In practice, round trip efficiency of over 45–60% has been forecasted for electrolysis units coupled to a nuclear power plant [8]."

The molten salts proposed for use in MSRs have high coefficients of thermal expansion, which leads to a large negative temperature coefficient of reactivity [2]. As the molten salt is heated in the core of a nuclear reactor it expands, increasing the average distance between the atoms of fissile material carried in the mixture, decreasing the probability of nuclear interactions, and thus lowering the rate of the fission reaction. Similarly, as the salt cools and contracts, nuclear interactions become more probable and the rate of the fission reaction increases. This makes an MSR more self-regulating and passively safe than an LWR. LWRs do experience this effect as well, but primarily in the water moderator between the fuel elements and, to a much lesser degree, the solid fuel elements themselves.

Maintenance of criticality within a moderated or reflected core is more passively safe in an MSR than it is in a typical LWR. Because the molten salt circulates the fuel throughout the entirety of the primary loop of the reactor, designs call for a core region where the mixture is made critical, while being subcritical everywhere else in the system. Such designs are beneficial from a safety perspective; in any situation where reactor conditions become dangerous, the fuel can be drained immediately into a subcritical containment and removed from the system. In contrast, the fuel in typical LWRs designs remains within the core at all times, and measures must be taken in accident scenarios to maintain criticality and manage reactor power.

The online removal of fission products from the system is possible through physical or pyrochemical processes. The potential for the continuous removal of neutron poison fission products, such as ^{135}Xe, is advantageous in the areas of neutron economy, reactor control, and the life of a single fuel loading. At the same time, removal of volatile chemical compounds formed from fission products helps in extending the life of the reactor systems physically exposed to the molten salt. All of this can be accomplished continuously while the reactor is operational. In contrast, LWRs must shut down entirely to open the core and refuel the reactor; refueling outages, which occur once per year on average, can result in up to $500,000 or more per day in lost revenue for a typical 1000 MW reactor [9].

Finally, unlike LWRs, there are no constraints on radiation damage that limit the achievable burnup of the fissile fuel in an MSR. LWRs must limit radiation damage to avoid excessive swelling of and structural damage to the fuel elements within the cladding.

Chapter 3: Computational Tools

3.1 Monte Carlo N-Particle

MCNP is a general purpose radiation transport code developed for the investigation of a wide range of nuclear-related problems. Its capability to create, track, and remove a range of simulated particles through a number of nuclear reactions makes it particularly suited to simulating problems in the areas of the fissioning and burnup of nuclear fuel, radiation shielding and dosimetry, radiography and medical physics, and the design of radiation detectors, particle accelerator targets, and nuclear fission and fusion reactors. The code is designed to simulate the time-dependent transport of particles across a continuous energy spectrum within any user-defined physical geometry.

The code utilizes Monte Carlo methods to determine a numerical solution to a simulated problem, repeatedly simulating the transport of large numbers of the particles participating in the nuclear process to be studied. Although the real process has a degree of randomness involved in how they interact with the environment, simulating large numbers of those particles that act in the same random fashion causes the problem to converge to a most probable, steady-state solution. MCNP simulations can be run to any desired accuracy, constrained only by the level of detail used in describing the geometry and physical composition of the model, the specified physics models or data tables to be used, and the quantity of particles used to statistically converge to the solution. The relation between the standard deviation in a measurement and the value of that measurement, which in this case is the number of the particles contributing to that measurement, is given by Knoll [10]:

$$\sigma = \sqrt{N} \tag{3.1}$$

which shows that as the number of particles, given by N, increases, the uncertainty in the measurement only decreases as $\sqrt{N}$, assuming that the quantity measured is distributed normally and that each particle has the same statistical weight. More illustrative of effect of the measured number of particles is the fractional uncertainty of the measurement, obtained by dividing Equation 3.1 by N:

$$\frac{\sigma}{N} = \frac{\sqrt{N}}{N} = \frac{1}{\sqrt{N}} \tag{3.2}$$

It can be seen from Equation 3.2 that increasing the number of particles contributing to the measurement, whether through increasing the measurement time, the efficiency of the detector in detecting the particles, or the intensity of the particle source will decrease the statistical uncertainty of the measurement. However, as shown from a plot of the equation in Figure 3.1, doing so results in diminishing returns. A measurement of 100 particles results in a statistical error of 10%, and increasing that number by a factor of 10 to 1,000 particles reduces the error to 3.2%, but a further increase by another factor of 10 particles only reduces the error to 1.0%.

In MCNP the user can specify the number of source particles to be used in a problem. Not all source particles will reach the specified detector regions, or tallies, so the number of particles necessary to

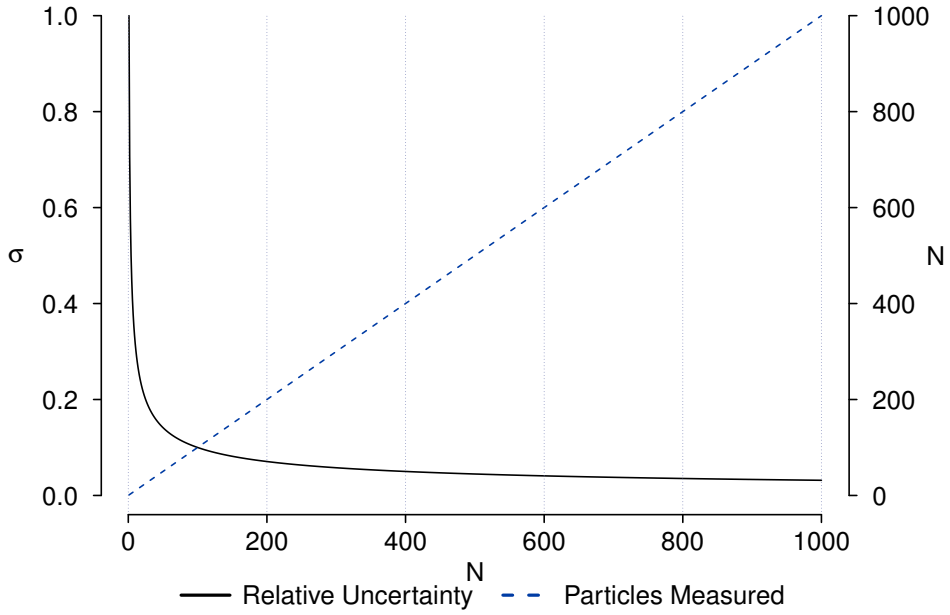

Figure 3.1: Statistical uncertainty as a function of the number of measured particles

achieve a desired uncertainty in a simulation may be far more than the number predicted by Equation 3.2. MCNP has variance reduction techniques that can be used to increase the number of particles reaching the detector regions, such as biasing particle directions or energies, adjusting particle statistical weights, or duplicating or removing particles entering specified regions. Variance reduction techniques can be used to reduce the computer time required to simulate a problem by reducing the proportion of particles that will not contribute to the problem tallies, hence saving wasted computer time.

MCNP is well suited for the majority, but not all, of the tasks related to the analysis of the MSNB neutronics. The code is designed to model static, unmoving systems; while the MSNB can be described as a static system at a single instant, which is useful for evaluating critical configurations or optimizing component designs, the operational system is dynamic. Thus, in the cases where modelling a dynamic system is more appropriate, approximations had to be made to investigate the system in MCNP.

3.1.1 Monte Carlo Methods

Monte Carlo methods utilize repeated random sampling within a modeled system to converge towards some expected value. These methods are particularly applicable in modelling systems that have many coupled degrees of freedom or are probabilistic in nature, but can be used to model wholly deterministic systems as well. In a generalized implementation, a model is constructed in which the expected value, which may be a combination of any number of contributing variables, is equivalent to the value of the real quantity to be determined. Simulation of the system then proceeds by sampling random numbers from distributions characterized by the state of each variable contributing to the model. The results of the sampling are then utilized within the model to produce the result of one iteration. The result of any single iteration can be any value, but results are biased towards an expected value by the combination of

the sampled distributions. By statistically combining the results of many iterations, the expected value approaches the physical quantity to be determined.

The results of random processes can be determined mathematically if they are simple, such as the probability of rolling a particular sum with a pair of dice, or uncoupled, like the probability of independently rolling a certain number with a die and landing a certain face on a coin flip. In cases involving thousands, millions, or more random coupled events, where the results of one random process determine which subsequent random process occurs, mathematical predictions become nearly impossible. This is the strength of Monte Carlo methods; by repeatedly simulating the same events and correctly sampling the correct probability distributions at each step, the most probable ultimate outcome emerges.

Monte Carlo methods became viable with the development of faster computers and means of efficiently producing sequences of acceptable pseudorandom numbers. Computers are best suited for highly repetitive, simple tasks. Monte Carlo methods are not difficult for computers to run, requiring only that a number is produced from a certain distribution, an event occurs based off of that number, a random number is produced for that event, which causes another event, and so on. This process must be repeated many times for as many particles as necessary.

In simulating random processes via Monte Carlo methods, it is essential that the distributions from which the pseudorandom numbers are taken are sampled correctly. For example, in the interaction between a neutron and an atom, a number of reactions can occur, including elastic or inelastic scattering of the neutron, absorption of the neutron, or the fissioning of the atomic nucleus. Any of the reactions can occur, but some are more probable depending on variables such as the relative energy of the neutron or the isotope of the atom involved. Thus, choosing a pseudorandom number from a probability distribution that reflects these favored reactions is essential to accurately recreate a physical process with a Monte Carlo method [11].

As a further example of the probabilistic nature of particle transport and the methods of simulating the process, the neutron transport equation, in the formulation given by Brown [12], is given in Equation 3.3:

$$\begin{aligned}\frac{1}{v}\frac{\partial\psi(\boldsymbol{r},E,\boldsymbol{\Omega},t)}{\partial t} &= Q(\boldsymbol{r},E,\boldsymbol{\Omega},t)\\ &\quad+\iint\psi(\boldsymbol{r},E',\boldsymbol{\Omega}',t)\;\Sigma_S(\boldsymbol{r},E'\to E,\boldsymbol{\Omega}\cdot\boldsymbol{\Omega}')\;d\boldsymbol{\Omega}'dE'\\ &\quad+\frac{\chi(\boldsymbol{r},E)}{4\pi}\iint\nu\Sigma_F(\boldsymbol{r},E')\;\psi(\boldsymbol{r},E',\boldsymbol{\Omega}',t)\;d\boldsymbol{\Omega}'dE'\\ &\quad-(\boldsymbol{\Omega}\cdot\nabla+\Sigma_T(\boldsymbol{r},E))\;\psi(\boldsymbol{r},E,\boldsymbol{\Omega},t)\end{aligned}\tag{3.3}$$

where the terms on the right side of the equation, in order by line, represent contributions to the neutron flux from an external source, scattering events, neutron multiplication, and losses due to leakage and collisions. Of particular note is the term $\chi(\boldsymbol{r},E)$, which represents the contribution of a probability density function to the energy distribution of produced fission neutrons and is itself dependent on the position $\boldsymbol{r}$ and energy E of the incident neutron. The terms Σ_T, Σ_F, and Σ_S represent various cross sections; are dependent on energy, position, and solid angle; and are inherently probabilistic as well. It

is this equation that is simulated in Monte Carlo problems involving neutron transport. In the course of simulating the problems, the random numbers used must be sampled from distributions matching those of the included probabilistic contributions in Equation 3.3.

To appropriately sample from the distributions describing the events to be simulated, it is necessary for Monte Carlo methods to utilize numbers from sequences of pseudorandom numbers whose properties approximate those of random number sequences. If there is any bias in the generation of the numbers used in the Monte Carlo simulations, there will be bias in the results. Some example methods for selecting pseudorandom numbers are given by Lux and Koblinger [11], which includes selecting values via the inverse distribution method, rejection techniques, or table lookups. MCNP uses random number generators to produce sequences of random numbers, which are then used to sample the correctly biased values from the necessary distributions through the inverse distribution method [13].

3.1.2 MCNP Input

An MCNP input file contains user-specified information necessary to completely describe a physical problem to be simulated, including the specification of the problem geometry, a description of the problem materials and cross-sections, particle source locations and characteristics, event tallies, and variance reduction techniques. The user can also specify other data as needed, such as the required physics models and data tables, simulation parameters, and output control. The data within the input file can be grouped into collections of cell definition cards, surface geometry cards, and data cards.

Surface cards are specified by the user to logically define the space occupied by a physical cell, and represent the boundaries between adjacent cells. The surfaces available to the user include infinite planes, cylinders, cones, spheres, and tori. Additionally, equations or collections of points can be used to define irregular surfaces. Various predefined macrobodies are also available, including parallelpipeds, hexagonal prisms, elliptical cylinders, truncated cones, or arbitrary polyhedrons. Each surface divides all space into two regions, and the entire geometry of the physical system can be described through combinations of any of the allowed surfaces.

Logical intersections and unions of the user-defined surfaces, and the complement of any other defined cells, are described in the cell cards to build the physical space partitioned by the surfaces. An example of the definition of three distinct regions in a two-dimensional physical space, delineated by two surfaces, is shown in Figure 3.2. The innermost area is defined as the region internal to surface 1, the outermost area is the region external to surface 2, and the intermediate area is the intersection of the regions external to surface 1 and internal to surface 2. The definition of cells in three-dimensional space in MCNP is achieved in a similar way.

No part of the physical space in an MCNP model can be left unassigned to a cell, and no two cells can overlap and share a region in space. A number of other parameters, both mandatory and optional, can be assigned to cells. Most essential is the designation of a material with which the cell is filled and the density of the filling material. The ability to set the importance of a cell for different particles is also useful; cell importances play an essential role in variance reduction by controlling the process of artificially duplicating or removing particles entering these regions. A number of other parameters for cells can be specified, including a defined cell volume, filling universe, or weight windows.

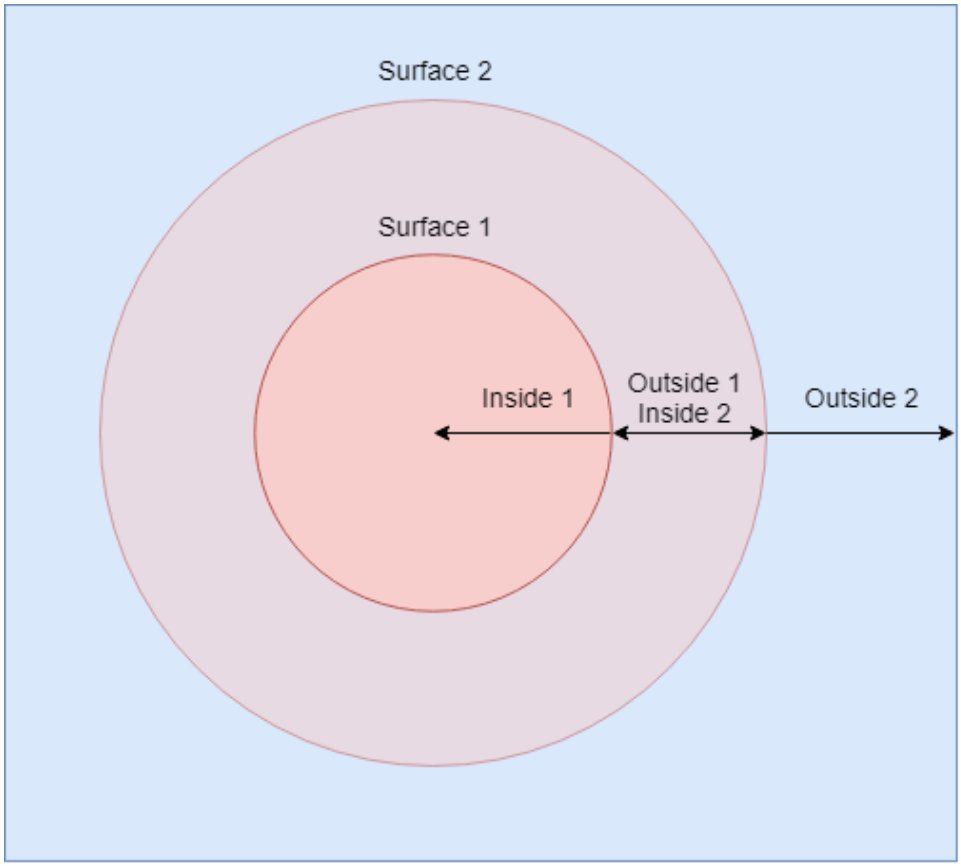

Figure 3.2: Logical cell definition in two dimensions

Data cards are used to define all of the properties and simulation parameters not defined in the surface and cell cards, including material compositions, particle sources, specific problem cards, tallies, physics models and tables, and variance reduction methods. This is by no means an exhaustive list of the possible definitions in the data cards, as MCNP allows for a great degree of control over a number of aspects related to the simulation.

3.1.3 KCODE Problem

MCNP uses the KCODE card to develop a criticality source that is used in determining k_{eff}, the effective neutron multiplication factor of a given system. Initial neutron source points specified by the user on the KSRC card are used to drive an initial round of fission events, which are then used as the source points of subsequent cycles. After allowing a sufficient number of cycles for the fission source points to stabilize to a steady state, the effective neutron multiplication factor of the reactor can be estimated. The user has control over several parameters relating to the convergence of the cycles, including the number of source particles per cycle, an initial guess for the value of the neutron multiplication factor, the number of beginning stabilization cycles to discard, and the total number of cycles to be run.

Equation 3.3 can be reorganized by grouping its terms as:

$$\frac{1}{v}\frac{\partial\psi(\boldsymbol{r},E,\boldsymbol{\Omega},t)}{\partial t} = Q + (S+M)\cdot\psi(\boldsymbol{r},E,\boldsymbol{\Omega},t) - (L+T)\cdot\psi(\boldsymbol{r},E,\boldsymbol{\Omega},t) \tag{3.4}$$

where Q is an external source term, S is scattering, M is multiplication, L is leakage, T is collisions, and ψ is the neutron flux. The first three terms, taken together, represent increases to the net number of neutrons in the system; the final terms represent losses. By assuming a fixed geometry and materials, no external source, and a steady-state, the equation can be reorganized into a static eigenvalue problem for solving fission multiplication problems [12]:

$$(L+T)\Psi_k(\boldsymbol{r},E,\boldsymbol{\Omega}) = \left(S + \frac{1}{k_{eff}}M\right)\Psi_k(\boldsymbol{r},E,\boldsymbol{\Omega}) \tag{3.5}$$

where Ψ_k is the neutron flux for problem history k. When simulating a KCODE problem, MCNP changes the factor $\frac{1}{k_{eff}}$ to adjust the relative strength of the fission source, balance the equation, and determine the steady-state solution.

KSRC should be used in conjunction with KCODE to specify initial source points for all discontinuous fuel elements, such as in the case of an LWR core containing assemblies of individual fuel pins. In this case, there is no guarantee that fission events would be triggered in every outlying fuel pin across the extent of the core, separated as they are by moderator and cladding. It was acceptable to specify only one source point in the model of the MSNB because of the single critical core region containing a continuous, homogeneously distributed fissile fuel. In this case, the initial cycles of the KCODE problem quickly develop into the desired fission sources throughout the core.

3.1.4 BURN Problem

MCNP uses the BURN card, along with a steady state neutron source determined by use of a concurrent KCODE card, to simulate the depletion of fissile fuel, the production of actinides and fission products, and the buildup of isotopes subsequently produced through the decay of the isotopes present. MCNP begins the burnup simulation by determining the system eigenvalue, neutron group fluxes, reaction rates, fission multiplicity, and recoverable energy per fission. These data are then fed to the CINDER90 subroutine, which performs the depletion calculation and returns the new materials and densities to MCNP for use in the simulation of the next burnup timestep.

The user can specify the level of detail desired in the fission product production calculation by choosing from several burnup tiers. The lowest level tier includes only a few of the most significant fission products, while the higher tiers include these and more. Computer time is significantly increased with the level of detail specified by the burnup tier. Table 3.1 shows the ranges of isotopes transported by MCNP within each burnup tier from a small selection of the available elements.

The isotopes in the chosen burnup tier are transported in addition to those listed on the material cards and those produced by the isotope generator algorithm, which only captures daughter reactions and a few other residual reactions. As a result, some isotopes may be present in the simulation results even if they were not explicitly specified in the material definitions and burnup tier. In specifying options on the BURN card, the user can also specify incremental timesteps to be used in the burnup problem, the reactor thermal power and power fraction applied to each timestep, and the materials in the MCNP

model to be burned.

Tier 1	**Tier 2**	**Tier 3**
^{131}Xe ^{134}Xe	^{124}Xe ^{126}Xe ^{128}Xe ^{129}Xe ^{130}Xe ^{131}Xe ^{132}Xe ^{134}Xe ^{135}Xe ^{136}Xe	^{123}Xe ^{124}Xe ^{126}Xe ^{128}Xe ^{129}Xe ^{130}Xe ^{131}Xe ^{132}Xe ^{133}Xe ^{134}Xe ^{135}Xe ^{136}Xe
^{133}Cs ^{137}Cs	^{133}Cs ^{134}Cs ^{135}Cs^{136}Cs ^{137}Cs	^{133}Cs ^{134}Cs ^{135}Cs ^{136}Cs ^{137}Cs
^{138}Ba	^{138}Ba	^{130}Ba ^{132}Ba ^{133}Ba ^{134}Ba ^{135}Ba ^{136}Ba ^{137}Ba ^{138}Ba ^{140}Ba
		^{138}La ^{139}La ^{140}La
		^{136}Ce ^{138}Ce ^{139}Ce ^{140}Ce ^{141}Ce ^{142}Ce ^{143}Ce ^{144}Ce
^{141}Pr	^{141}Pr	^{141}Pr ^{142}Pr ^{143}Pr

Table 3.1: Sample of fission product contents within each MCNP burnup tier

Chapter 4: Methods and Procedures

The investigation into the properties of the MSNB in the areas of criticality, burnup, and radioactive dose was accomplished primarily by simulating the system in MCNP. The MCNP model of the MSNB was developed to a high degree of accuracy to fully simulate a wide range of physical effects, including: the criticality of salt circulating outside the core, the effects of varying salt temperature, and the effectiveness of the reflecting and absorbing materials in the reactor, among others. While the added complexity of the model generally increased the computer time required to complete a simulation, several effects were discovered that were not present in previous, simplified MCNP models. In some cases the ORIGEN code was used to provide inputs to MCNP, further process MCNP output, or provide concurrent results to be compared to those produced by MCNP. ORIGEN was used mainly to verify fission product quantities and determine energy-binned neutron and photon fluxes emitted by the MSNB following its operational period. A rendering of the MSNB is shown in Figure 4.1.

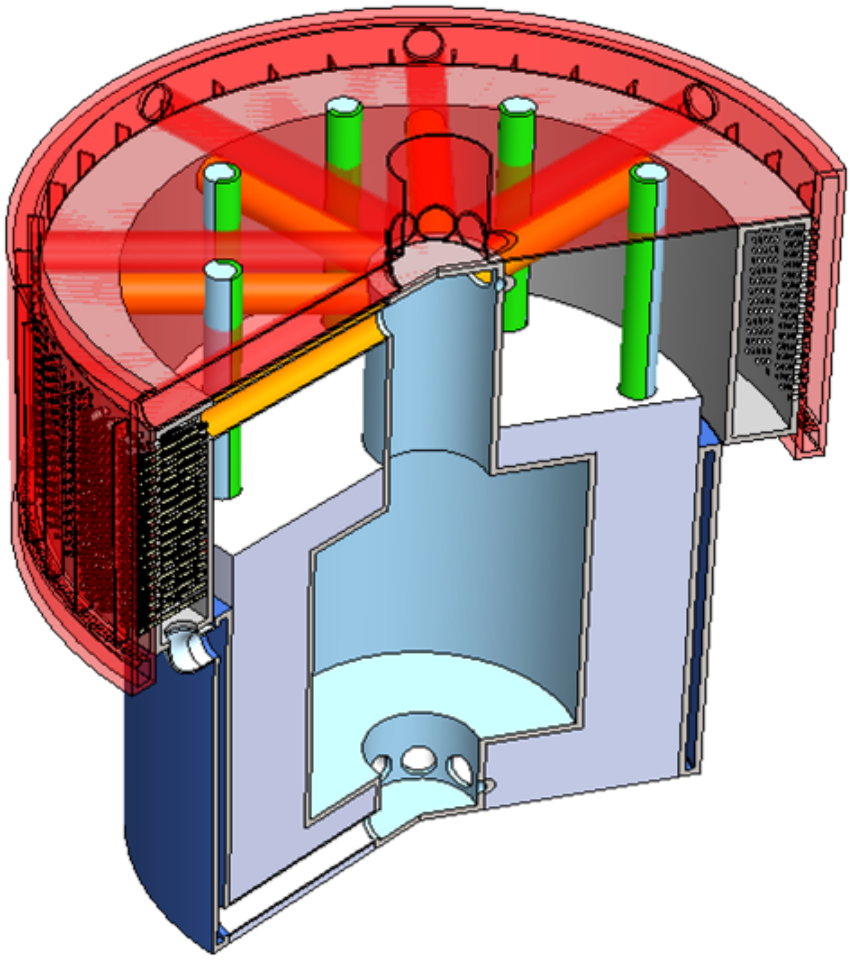

Figure 4.1: Rendered model of the MSNB

4.1 Material Selection and Characterization

4.1.1 Neutron Attenuation and Moderation

Proposed materials for the neutron reflector were simulated in MCNP to determine the thickness to which neutrons across the entire energy spectrum would be able to penetrate. The results of the MCNP simulations were used to inform MSNB design decisions, including the necessary dimensions and geometry of the reflector and the location of the control rods. Optimization of the reflector material and thickness was necessary to limit the overall size of the reactor and conform to a reactor configuration that enabled circulation by natural convection, while retaining the desired operational capabilities. The materials investigated were reactor grade graphite and beryllium-containing compounds, specifically pure beryllium metal and Beryllium Oxide (BeO). The neutron reflector in this case simultaneously acts as a moderator, with the elastic collisions reflecting neutrons back into the core also reducing their kinetic energy into the thermal spectrum. To promote these effects, the bulk of the material must be composed of low mass isotopes, with masses closer to that of an incident neutron more effectively moderating its energy, and have as low as possible an absorption cross section across the neutron energy range.

The penetration depth of neutrons in hafnium, the neutron absorber chosen for use in the absorbing plates embedded in the control rods, was also investigated to determine the minimum thickness of hafnium required to effectively attenuate the neutron flux and control the fission reaction. Minimizing the thickness of the hafnium plates in the control rods simultaneously increased the amount of reflecting material available in each rod and, consequently, the reactivity worth of each.

Finally, neutron fluxes through various thicknesses of the FLiBe-UF_4 eutectic were simulated. Because of the significant faction of beryllium making up the elemental composition of FLiBe, the salt is itself a significant neutron moderator. The MCNP simulation was performed to determine the volume of material required for the neutrons to be moderated without the use of any external reflecting material, inform design decisions regarding the dimensions of the core of the reactor, and investigate the potential for the eutectic to reach criticality outside of the MSNB core.

In each case the material was simulated as a series of concentric cylinders of 0.1 cm thickness, starting at 5.0 cm and extending to between 25.0 cm and 45.5 cm, depending on the material. Each cell was filled with the test material at a uniform density. A neutron source was placed at the center of the arrangement of cylinders and set to emit neutrons isotropically across an energy spectrum from 10^{-4} eV up to 20 MeV, with a uniform distribution of neutrons across the energy range. Each simulation used 10,000,000 particles to ensure an even distribution of incident neutron energies and reduce statistical uncertainty. The neutron importance in successive cells was increased as the inverse of the anticipated decrease of the particle flux to maintain an approximately constant flux throughout the model. Neutron fluxes were measured at the surfaces defining the boundaries between each cell and were divided into energy bins analogous to those of the neutron source energies.

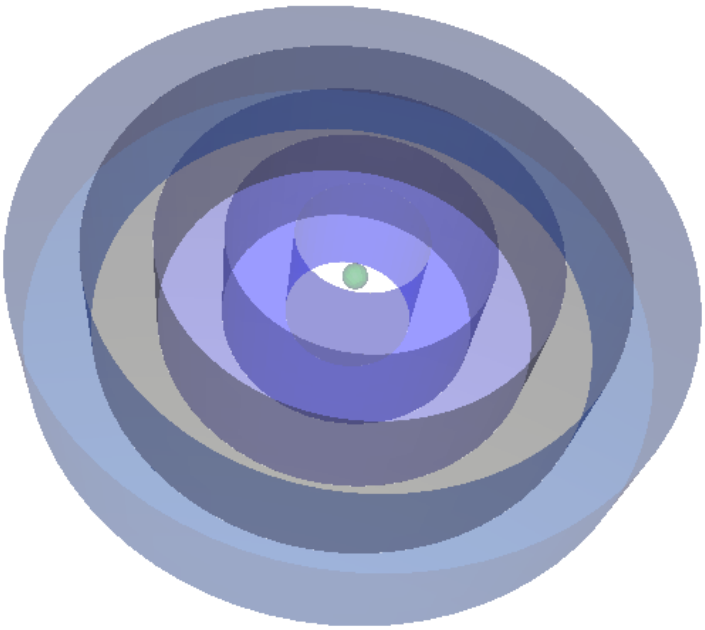

Figure 4.2: Cutaway of the neutron attenuation simulation of MSNB materials

4.1.2 FLiBe – Uranium Hexafluoride Density and Composition

Specification of a material density is required for MCNP simulations, and differences in densities can have dramatic effects on the simulation results. The density of FLiBe and UF_4 have been experimentally determined under a number of varied conditions, and correlations exist that characterize the dependence of density on temperature. However, no data exists for the eutectic mixture in the proportions used in the MSNB. In the absence of this data, the density of the mixture was estimated using the formula given by Felder and Rousseau [7]:

$$\frac{1}{\bar{\rho}} = \sum_{i=1}^{n} \frac{x_i}{\rho_i} \tag{4.1}$$

where $\bar{\rho}$ is the density of the mixture and x_i and ρ_i are the mass fraction and density of the ith component of the mixture, respectively. Equation 4.1 represents the weighted average of each of the components of a mixture, with the components constituting a greater fraction of the total mass contributing a correspondingly greater faction to the combined density. Using this formula, the individual densities of FLiBe and UF_4 can be combined to provide an estimate of the density of the mixture used in the MSNB. It should be noted, however, that Equation 4.1 assumes that the molecular structures of the components of the mixture are similar and that the volumes of the individual components are additive; i.e., the sum of the volumes of each component is equal to the volume of the mixture.

It was assumed that the UF_4 remained at a constant density, again due to a lack of available data on the density of UF_4 in the range of temperatures expected in the MSNB. Thus, a density of 6.7 g·cm^{-3} was used in all subsequent calculations. Ignatev et al. determined a correlation for the density of FLiBe

as a function of temperature given by [14]:

$$\rho = 2.163 - A(T - 601.4),$$
$$\text{with } A = \begin{cases} 4.06 \cdot 10^{-4}, & T \leq 700°\text{C} \\ 6.87 \cdot 10^{-4}, & T > 700°\text{C} \end{cases} \tag{4.2}$$

where T is the FLiBe temperature in Celsius and ρ is given in g·cm^{-3}. The combination of the assumed constant UF_4 density and the temperature-dependent FLiBe density obtained from Equation 4.1 yielded a temperature-dependent density correlation for the mixture at any ratio of FLiBe to UF_4. The correlation allowed for the simulation of temperature-related effects on the fuel of the MSNB. For example, a recreation of the temperature gradients increasing across the height of the core and decreasing through the upper heat exchanging annulus was made possible. This enabled investigations of reactivity and neutron flux changes in accordance with the temperature effects discussed in Section 2.1.2. Investigations into the effects of excessive reactor temperatures in accident scenarios were also enabled by the use of this correlation.

Neutron data libraries provided with MCNP were used with ^{235}U and ^{238}U to ensure accurate simulation of the nuclear processes associated with these isotopes. The provided libraries have temperatures at which the data were evaluated; using those libraries with evaluation temperatures closest to the expected local temperature within the MSNB allowed for the most accurate simulation of the system. The two data libraries closest to the anticipated operating temperature range of the system are listed in Table 4.1.

Library Name	**ZAID Suffix**	**Temperature (K)**	**Temperature (°C)**
endf62mt	.16c	800.00	626.85
endf62mt	.17c	1200.00	926.85

Table 4.1: Neutron data libraries used for ^{235}U and ^{238}U in MCNP simulations

The midpoint between the evaluation temperatures of these two libraries is 776.85°C. Regions within the reactor expected to remain under the midpoint temperature, including the lower regions of the upper annulus, lower annulus, incoming spokes, and lower riser and core used the .16c ZAID suffix. The remaining high temperature regions, including the upper riser, outgoing spokes, and upper regions of the upper annulus used the .17c ZAID suffix. Specification of unique data libraries for the same isotopic components of the same material in different locations required multiple definitions of the eutectic across multiple M cards, with only these libraries changed between the definitions. Repeated definition of the eutectic was also necessary for simulating the burnup of the same material at different densities, discussed in Section 4.4.

The composition of the FLiBe-UF_4 eutectic for the definition of the material in MCNP was described in terms of the relative weight of the elemental components. MCNP can interpret fractions of elemental constituents in materials as either weight fractions or atom fractions; utilizing weight fractions simplified

calculations of the density as the fuel loading of UF_4 within the FLiBe was changed. Table 4.2 lists the isotopes and mass fractions used in the definition of the FLiBe-UF_4 eutectic at 7% UF_4 by weight and at 20% ^{235}U enrichment.

Isotope	**ZAID**	**Mass Fraction**
^{7}Li	3007	0.27114
^{9}Be	4009	0.13557
^{19}F	9019	0.58309
^{235}U	92235	0.00204
^{238}U	92238	0.00816

Table 4.2: Isotopic constituents of the FLiBe-UF_4 eutectic

4.2 Criticality Control

4.2.1 Delayed Neutrons

Before simulations related to the criticality of the system were attempted in MCNP, the suitability of the code for simulating the system had to be established. The vast majority of the neutrons produced by the fissioning of ^{235}U nuclei are prompt neutrons, which are emitted on the order of 10^{-13} s from the fission event. With respect to modeling a liquid fuel system dominated by these neutrons, and given a flow rate on the order of centimeters per second through the core, the system can be treated as static; the fuel will have not moved appreciably between the fission event and the production of the prompt neutrons. However, a small fraction of the neutrons originate from unstable daughter products of the initial fission, and can be delayed in their emission by up to several tens of seconds. For these neutrons it is entirely possible that between the occurrence of the initial fission event and their eventual emission, the decaying fission product responsible for their production could have left the core. These neutrons would then be considered lost and not contributing to the ongoing fission chain reaction. If the fraction of delayed neutrons lost in reality is significant, then simulation of the MSNB as a static system within MCNP would overestimate the criticality of the reactor and be unsuitable as a tool for further investigation. A simple study was conducted to determine the expected change in the average delayed neutron lifetime and abundance expected in the MSNB system as a result of fission daughter products leaving the core. Table 4.3 lists six neutron groups, given by Lamarsh, with their half lives, lifetimes, and abundances [15].

The average lifetime across these groups, weighted by the relative abundance of each, is 13.02 seconds. The delayed neutrons described by these events constitute 0.65% of all neutrons created through ^{235}U fissions. To determine how these data change in a dynamic system, 1,000,000 fission events were initiated at random positions within the MSNB core volume, creating neutrons with the relative abundances listed in Table 4.3. Given the flow rate of 560 gallons per minute through the core, corresponding to a fluid velocity of 0.0247 m/s, it was then determined whether each neutron produced by a delayed neutron precursor would do so inside the core volume. The fraction of delayed neutrons lost to the non-core

Group	$\mathbf{T}_{1/2}$	**Abundance**	**Lifetime (s)**
1	55.72	0.000215	2.658
2	22.72	0.001424	7.179
3	6.22	0.001274	1.758
4	2.30	0.002568	1.311
5	0.61	0.000748	0.101
6	0.23	0.000273	0.014

Table 4.3: Delayed neutron group half lives, abundances, and lifetimes

volume was used to determine the effective average lifetime and useful delayed neutron fraction.

4.2.2 Control Rod Design

Active control of MSNB criticality is achieved with an arrangement of control rods, embedded in the neutron reflector and equally spaced around the core as shown in Figure 4.3. Each control rod is composed of a neutron reflecting core material and a neutron absorbing plate affixed to one third of the control rod circumference. Rotation of the control rods inwards towards the core exposes a greater fraction of the absorbing plate to the neutron flux within the reflector, which reduces the overall neutron flux and lowers the effective neutron multiplication factor of the system. Similarly, rotating the absorbing plates away from the reactor core, and exposing more of the reflecting core of the control rods, increases the effective neutron multiplication factor.

The control rods were each defined within MCNP as logical combinations of two concentric cylinders and two vertical planes. The planes, intersecting at the center of the cylinders and having a 120°angle between them, were used to define the edges of the neutron absorbing plates embedded in the control rods. The bulk of each control rod, made up of the neutron reflector, was defined as the union of the entirety of the inner cylinder and of the volume of the outer cylinder not enclosed between the intersecting planes. The absorbing plate was then defined as the intersection of the volume outside the smaller cylinder, the volume inside the larger cylinder, and the region enclosed by the intersecting planes.

The sense of the plane surface, used in the definition of cells, is typically determined by whether the region of space delineated by the plane contains the origin of the system, or by another set of rules if the origin lies in the plane. To rotate the control rods by redefining each of the plane pairs in a new orientation would necessitate changing the cell definitions of the control rods and absorbing plates whenever the updated surface passed through the origin. To circumvent this complication, a transformation TR card was applied to each pair of planes, which allowed for a two-dimensional rotation θ about the z-axis to be applied, using the following matrix:

$$R_z = \begin{bmatrix} \cos\theta & -\sin\theta & 0 \\ \sin\theta & \cos\theta & 0 \\ 0 & 0 & 1 \end{bmatrix}$$

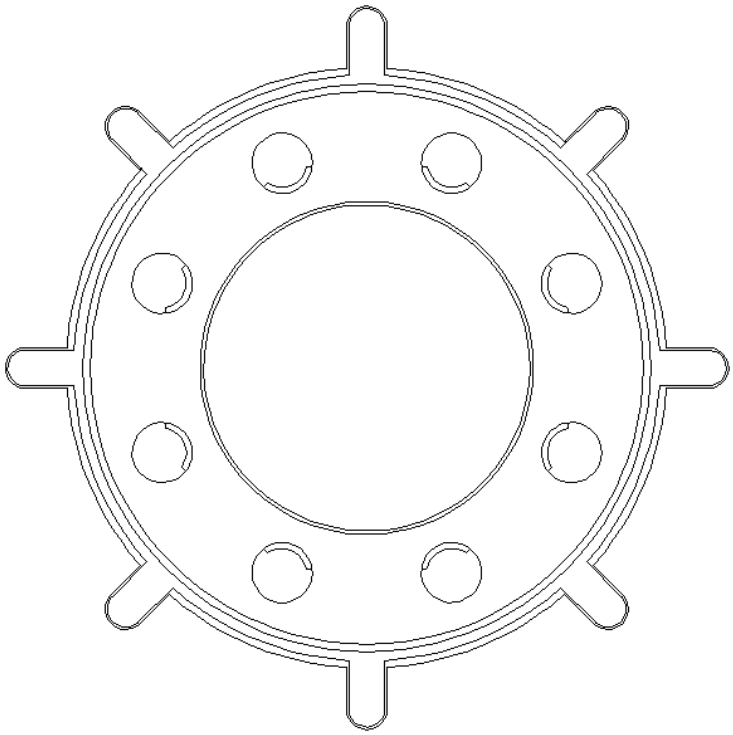

Figure 4.3: Cross section of the MSNB as viewed from above

Rotation of the control rods within the MCNP model was then achieved by simply calculating the elements of the rotation matrix for a given θ for each transformation card; no adjustments to the logical definitions of the control rods and plates was required because the sense of the plane regions was determined before the transformation. However, the rotations applied by the transformation card are performed relative to the origin of the system, which would cause each plane pair to follow an arc around the origin rather than simply rotate in place. This was circumvented by simply defining the planes at the origin of the system, because the transformation card simultaneously allows for the specification of a rotation and displacement. By defining the planes at the origin, the correct rotation could be applied, after which the coordinates of the center of each control rod could be specified to simultaneously move them to the correct final position.

To optimize the performance of the control rods, a sensitivity analysis of all combinations of control rod radius, distance from the core, and neutron absorbing plate thickness was conducted in MCNP. The most optimal design was expected to have the largest radius, be located the farthest from the core, have the thinnest absorber plate, and be able to bring the neutron multiplication factor below unity with the rods fully rotated inward. The first three parameters all serve to increase the criticality of the reactor, and correspondingly the operational period of the reactor. In the case of the total control rod diameter, a larger control rod allows the plates to be rotated into a position farther away from the core, because the distance between the closest and farthest positions is equal to the diameter of the control rod. At the same time, a greater volume of reflecting material is placed between the core and the absorbing plates in the extreme position, further increasing the criticality of the system. Placing the control rods farther

away from the core increases the distance from the core to both of the extreme positions of the neutron absorbing plates. Finally, reducing the thickness of the absorbing plates ensures that only as few neutrons are eliminated as necessary to halt the nuclear reaction. Optimization of these parameters was essential to ensure successful reactor operation through the entire reactor period. Because of the rotating control rod design, the neutron absorbing plates are always active within the system. Thus, minimizing their effects by placing them at the most extreme location possible is essential to limit their undesirable effects on the neutron economy, particularly near the end of the operational period when the quantity of fissile fuel available to drive the nuclear reaction is lower.

The ranges of the parameters used in the sensitivity analysis, informed by the results of the materials study discussed in Section 4.1.1, are listed in Table 4.4:

Parameter	**Minimum (cm)**	**Maximum (cm)**	**Step Size (cm)**
Distance, Center to Center	85.00	95.00	2.50
Radius	1.00	15.00	1.00
Neutron Absorber Plate Thickness	0.25	7.50	0.25

Table 4.4: Control rod sensitivity analysis parameters

After determining the optimal configuration of the control rods, the performance of the design across the full range of rotated positions was evaluated in MCNP. The design was implemented in a model with a full fuel load and simulated in a KCODE problem. The control rods were rotated in 0.25 degree increments between the two extreme positions, and the value of the effective neutron multiplication factor was recorded at each step.

The response of the reactor to having every control rod entirely removed from the system at the beginning of operation was also investigated. A beginning of life model, with the loading of fissile fuel at its highest concentration at any point during operation, was used as both a most conservative case and for the investigation of a plausible scenario, such as could occur during transport of the MSNB prior to installation. The materials defined for the control rods and absorber plates in the MCNP model were each replaced with air, with an elemental composition and density given by McConn, Gesh, Pagh, Rucker, and Williams [16]. The typical KCODE problem was run with the MSNB in this configuration. It was expected that the effective neutron multiplication factor would decrease with the removal of the substantial volume of neutron reflecting material contained in the control rods, but it was unknown whether this would overcome the increase in the neutron multiplication factor caused by the simultaneous removal of the neutron absorber. Given that the value of the effective neutron multiplication factor predicted by MCNP was greater than unity when the control rods were rotated fully outward in the beginning of life model, it was unknown whether the combination of these effects would render the reactor subcritical. Similar simulations were conducted to investigate the effects of the replacement of the control rods with water and solid neutron absorbing materials.

4.2.3 Miscellaneous Criticality Effects

In an accident scenario that results in a rapid increase in the temperature of the FLiBe-UF_4 eutectic, such as a loss of cooling in the secondary loop or the system reaching a supercritical configuration, it is essential to understand how the nuclear characteristics of the MSNB will change in response. Using the density of the eutectic determined by application of Equation 4.1, the material was simulated at different temperatures in the MCNP model. However, it should be noted that changing the density of the material does not account for other effects related to the increase in temperature, such as thermal Doppler broadening of the neutron absorption spectrum of ^{235}U. The use of different neutron data libraries was used to a small degree to properly simulate other thermal effects, as discussed in Section 4.1.2, but there were few libraries evaluated at the necessary temperatures. Thus, the simulated temperature of the eutectic in the simulated system was mainly increased by lowering the density in accordance with Equations 4.1 and 4.2. The relative temperature gradients within the system, particularly the gradients within the core and the upper annulus, were maintained; all of the densities were increased uniformly. Temperatures were simulated in the range of 600°C to 1200°C at the core inlet, corresponding to outlet temperatures between 700°C and 1300°C.

High fidelity modeling of the MSNB revealed several unexpected effects. Preliminary designs for the reactor called for conventional control rod designs, which were composed entirely of neutron-absorbing material and moved vertically within the reactor. Simplified MCNP simulations of the reactor at this stage consisted of these control rods embedded in a neutron reflector that entirely encapsulated a solid cylinder of the eutectic mixture. In this model and with this control rod design, control of the fission reaction was achievable. When the change to the control rod design was made, and more detailed models of the system were developed, control of the fission chain reaction was lost. Even in the extreme case of the control rod design, where a neutron absorber made up half of the volume of each rod, the effective neutron multiplication factor could not be reduced below unity. It was discovered that, in developing the high fidelity model of the reactor, fissile fuel was now present in locations outside of the core, particularly in the downcomers immediately outside of the reflector. In this case, rotation of the control rods into the position that fully exposed the neutron absorber to the core exposed a corresponding volume of neutron reflector to the fuel outside of the core, which was enough to maintain the total neutron multiplication factor of the system. After adding a relatively impenetrable neutron barrier on the outside of the reflector, criticality control was restored.

4.3 MSNB Core Neutron Flux

Characterization of the neutron flux through the MSNB core was achieved through simulation in MCNP, again using the KCODE card to reproduce the distributed fission neutron source present in the operation of the real reactor. Determination of the neutron flux throughout the entirety of the core was essential to calculate an average neutron flux and energy spectrum for use in radiation dose simulations. Additionally, simulation of the neutron flux represented an opportunity to verify that the system was behaving as expected and investigate any unexpected effects.

Because of the symmetry of the MSNB system, due to the regular angular spacing of the control

rods and upper and lower eutectic-distributing spokes, it was only required that one eighth of system be simulated. It was assumed that each symmetric region would behave similarly, so a finer spatial resolution, more precise simulation results, and decreased computer time could be achieved by simulating only a fraction of the MSNB core. To evaluate the spatially varying flux throughout the core, 100 point detectors were arranged in an equally spaced grid and at a uniform height within the symmetric region. Among the tally cards available in MCNP to determine particle fluxes, only the F5 point detector tally returns spatially dependent information; the remaining tallies report results averaged over surfaces or cells. Multiple simulations were carried out with the same equally spaced grid at different heights to fully characterize the neutron flux through the core volume. The height differences between the simulation layers was equal to the distance between adjacent detectors within the same layer to produce, with all of the independent simulations taken together, a cubic grid of point detector results throughout the MSNB core. A visualization of one layer of the point detector grid within the symmetric region of the core is shown in Figure 4.4. The detectors were constrained within a region subject to the following inequalities:

$$\begin{aligned} \sqrt{x^2 + y^2} &< R \\ 0 \leq \arctan\left(\frac{y}{x}\right) &\leq \theta \end{aligned} \tag{4.3}$$

where x and y are the coordinates of a given point detector, R is the radius of the MSNB core, and θ is the angular width of the symmetric region. Within the 45° symmetric region, Equation 4.3 allowed points to fall on the boundaries at 0° and 45°, but not at the edge of the core at radius R. The reason for this is that the boundaries at each angle are chosen independent of the MCNP model, but the radial boundary coincides with a bounding surface in the model and can give inaccurate results if a point detector is placed there. The spacing between adjacent points was chosen such that, subject to the constraints in Equation 4.3, 100 point detectors were used because the F5 tally limits the number of detectors in one tally definition to no more than 100. The use of a square grid of point detectors constrained within the cylindrical core resulted in irregular arrangements of detectors near the edges of the core. However, the otherwise regular spacing of the detectors allowed for a simple mapping of the results to the entirety of the core which would not be possible with other arrangements of detectors.

The definition of the KCODE card involved 10,000 source neutrons per history, 50 initial histories to be skipped, and 100 subsequent tally-contributing histories. Flux tally energy bins were specified corresponding to the Joint Evaluated Fission and Fusion (JEFF) Nuclear Data Library neutron energy 252 group structure given by the Nuclear Energy Agency [17] because the simulation data were used primarily for fission product production in ORIGEN, which used the JEFF-3.0/A Nuclear Data Library.

The mean free path of a neutron in the FLiBe-UF_4 eutectic material was used to specify the radius of a sphere of exclusion for each point detector. This zone is used by MCNP to ignore repeated flux-related events that may be caused by the same neutron and would lead to an overestimation of the flux. The MCNP6.2 User's Manual recommends that the radius of the sphere should be between 1/8 to 1/2 of the mean free path for neutrons of average energy [13]. The mean free path can be calculated as the inverse of the total macroscopic cross section of a material. In the case of the FLiBe-UF_4 eutectic, the mean free path was determined to be 1.50 cm, with the radius of the sphere of exclusion then specified as 0.75 cm.

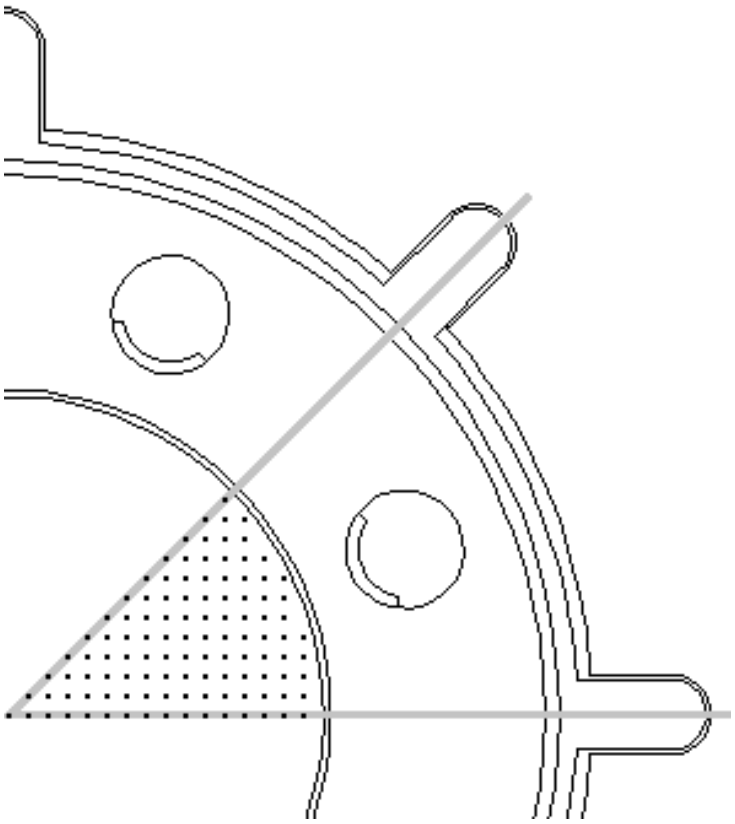

Figure 4.4: Arrangement of point detectors within a symmetric section of the MSNB

4.4 MSNB Operation

After developing the system design required to achieve an initial critical configuration, the behavior of the MSNB during and following the operational period was investigated. MCNP was primarily used to determine whether a specific fuel loading, enrichment, and reactor configuration would be sufficient to operate at the specified power for the desired operational period. The primary means of investigation was through successive executions of MCNP BURN problems, where the output of one problem was incorporated into the input of the next alongside necessary adjustments to the reactor configuration. While the BURN card provides functionality for completing multiple successive timesteps at specified operational powers and with limited adjustments to the problem geometry and material compositions, this functionality was not sufficient for simulating a system such as the MSNB. In particular, neither rotation of the control rods to maintain system criticality or alterations to multiple problem materials is possible. To provide this necessary functionality, MCNP was controlled through an external script.

Before initiating the script, the user must specify the initial reactor configuration. This primarily involves defining the MCNP material cards for the eutectic mixture to reflect the desired ^{235}U enrichment and ratio of UF_4 to FLiBe. A first guess at the necessary position of the control rods to achieve initial criticality is also required. Various other parameters related to the simulation are defined at this time, including the number of source particles and histories to be used for KCODE and BURN problems; the

timesteps to be simulated; maximum reactor power and, if desired, the fraction of the power to be used at each timestep; the MCNP fission product tier; any isotopes to be managed between simulation timesteps; the angular step size to be used when adjusting the control rod positions; and the tolerance that the neutron multiplication factor must fall within. The algorithm implemented by the script then proceeds through the following steps:

1. The script creates and runs an MCNP input file from the specified initialization data. This input file executes a KCODE problem to determine the effective neutron multiplication factor of the system given a particular reactor configuration.
2. The MCNP-generated output file is read by the script and the value of the neutron multiplication factor is returned.

   (a) If the value of the neutron multiplication factor is greater than unity and within the user-specified tolerance, continue to the next step. The same MCNP input parameters, including the composition of the eutectic and the position of the control rods, are used in any subsequent MCNP input files created in this iteration.

   (b) If the value of the neutron multiplication factor is less than unity or greater than the user-specified tolerance, the script returns to Step 1. The angular step size applied to the control rod position is adjusted depending on a comparison of the returned value of the neutron multiplication factor and the value returned in the previous attempt, if any. For example, if the previous value was less than unity and the current value was much greater than unity, the size of the rotation step is reduced. The updated rotation step is then applied to the control rod position of the previous iteration.

3. The script creates and runs an MCNP input file using the control rod positions required to achieve criticality, determined in Step 2. This input file executes a BURN problem to simulate the burnup of fissile fuel and the buildup of fission products through fissions and decays. In the case that an isotopic component present in the eutectic, added by the script from a previous timestep, does not have the required data in the MCNP data libraries to be included in the BURN problem, MCNP will produce a fatal error. In this instance, the script will read the output file to determine the isotope that produced the error, add it to the list of isotopes to be emitted from the transport calculation via the OMIT option on the BURN card, and attempt to run the input file again.
4. The MCNP-generated output file is read by the script and the isotopic constituents of each eutectic material at the end of the BURN timestep are returned. The mass fractions of any isotopes specified by the user in the initialization step are set to a specified value or removed entirely. The mass fractions of the eutectic constituents are then normalized, appended with any necessary neutron data libraries, and then saved as the material to be used for the eutectic in the next timestep. The control rod orientation used in the timestep is rotated inward by the angular step size and used as the first guess at the next control rod position. This was done to avoid the position of the control rods steadily rotating outwards due to the inherent uncertainty in the results of the MCNP simulation, and the tendency of the script to only adjust the orientation in one direction in a given timestep.

5. If there are remaining timesteps to be simulated, the script returns to Step 1.

Controlling the creation, execution, and evaluation of the MCNP through an external script allows absolute control over the model, provided the script can be configured to reliably make the needed changes. The fuel burnup and inventory of produced fission products predicted by MCNP were used to inform subsequent operational simulations, particularly in the specification of the initial ratio of UF_4 to FLiBe, in order to reach the desired operational requirements.

4.4.1 Fuel Burnup

The burnup of the fuel, represented by the difference in the mass of the ^{235}U inventory between startup and shutdown, was determined in the course of simulating MSNB operation with the MCNP BURN card. In the process of creating an MCNP input template for the dynamically generated input files and configuring the script to create these files, several issues needed to be considered.

MCNP does not allow for the same material to appear at different densities in multiple cell definitions if it is specified to be burned on the BURN card. To circumvent this, multiple identical definitions of the FLiBe-UF_4 eutectic material were created, corresponding to the number of unique densities needed in the model. Because of the close relationship between the varying density and temperature of the material, the repeated definitions also allowed for the use of different neutron data libraries which were evaluated at the corresponding temperatures. This solution ensured the most accurate simulation of the reactor operation and burnup, but also complicated the process of reading the results of each burnup timestep and reincorporating the results into the model for the next timestep. MCNP does, however, provide a table in the output file that lists the sums of the components of each burned material; so long as the FLiBe-UF_4 eutectic was the only material burned, the data from this table could be used.

The volumes of defined cells and the density of the materials with which they are filled are used by MCNP to determine the total mass, and the number of atoms, of each specified nuclide in the system. The volumes of rotationally symmetric or polyhedral cells can be calculated automatically by MCNP, but the more complicated cells included in the MSNB model required manual calculation and specification within the input file. The dependence of the code on the density of the material, in conjunction with the volume, again highlights the importance of the calculated density of the mixture as discussed in Section 4.1.2. The density of the eutectic not only influenced the instantaneous criticality of the system through the inter-atomic spacing of the fissile fuel, but also the calculation of the number of fissile atoms included in the simulation.

4.4.2 Fission Product Production

As part of the simulations of MSNB operation and burnup, the quantities of fission products and actinides produced within the system were tracked. Because the MSNB operates as a closed system, the quantities of these nuclides are governed by the following differential equation [18]:

$$\frac{\partial N_i}{\partial t} = \sum_{j \neq i} \left(l_{ij} \lambda_j + f_{ij} \sigma_j \phi \right) N_j \left(t \right) - \left(\lambda_i + \sigma_i \phi \right) N_i \left(t \right) + S_i \left(t \right) \tag{4.4}$$

where N_i is the quantity of nuclide i, λ_i is the decay constant of nuclide i, l_{ij} is the fractional yield of nuclide i from the decay of nuclide j, σ_i is the spectrum-averaged removal cross section for nuclide i, f_{ij} is the fractional yield of nuclide i from neutron-induced removal of nuclide j, ϕ is the time-dependent neutron flux, and S_i is a time-dependent source term. Equation 4.4 represents the balance of the nuclear processes simulated by MCNP and the CINDER90 subroutine, as well as the ORIGEN code, to track the production and loss of fission products and actinides during operation.

The choice of the fission product burnup tier to be used in the simulation had a significant influence on the result. One consequence of note is the relation between the choice of burnup tier and the required computation time. As the complexity of the tier and the number of isotopes to be tracked increases, there is a corresponding increase in the computational time required to complete a simulation timestep. The choice of the burnup tier required balancing the computational time available, the minimum size of the simulation timesteps, and the desired accuracy in the determination of the fission products produced. To meet these needs the second burnup tier was used for the majority of the simulations, although the first, and most simple, tier was used in some simulations involving relatively small timesteps.

In addition to the simulations of MSNB operations in MCNP, the system was simulated in ORIGEN to provide results in parallel for comparison. Because of differences in the functionality of each code and in the models used, some results from one code were treated as more reliable than those from the other. MCNP excels at particle transport and criticality evaluation, allows for a comprehensive user-specified problem geometry, and can determine its own particle source terms, but does not have exhaustive data corresponding to fission product production and decay. ORIGEN has extensive data relating to the production of fission products, but requires an explicitly defined particle source and does not allow for the specification of a problem geometry. The ORIGEN simulations also provided data regarding the ingrowth and decay of radionuclides following reactor shutdown.

The parallel simulation in ORIGEN used the nuclide masses calculated by MCNP at the start of the burnup simulation as the material to be irradiated. Using the quantities reported by MCNP, as opposed to manual calculations of the masses of each material component, ensured that each simulation started with the same inventory of radionuclides. Because of the inability to specify a highly detailed geometry and extract data relating to the individual physical structures within the reactor, the ORIGEN model only included the FLiBe-UF_4 eutectic material.

Simulation of the burnup and production of fission products in ORIGEN required the definition of a total neutron flux and the energy distribution of the particles making up that flux. This data was calculated from MCNP simulations of the neutron flux in the MSNB core, the results of which were averaged to produce an average value for the flux as well as the average energy distribution. The energies ranged from $1.0 \cdot 10^{-4}$ eV to 20 Mev, corresponding to the 252 group structure used in JEFF-3.0/A [17] to make use of the data provided by the library.

The entire simulation spanned MSNB operation through two distinct states: an operational case in which the reactor materials were irradiated by the user-defined neutron flux, and a cooldown case in which no neutron flux was applied and the quantities of radionuclides changed only through ingrowth and decay. Because of the abrupt changes in neutron flux that occurred at reactor startup and at the transition between the two operational cases, smaller timesteps were used around these times to ensure

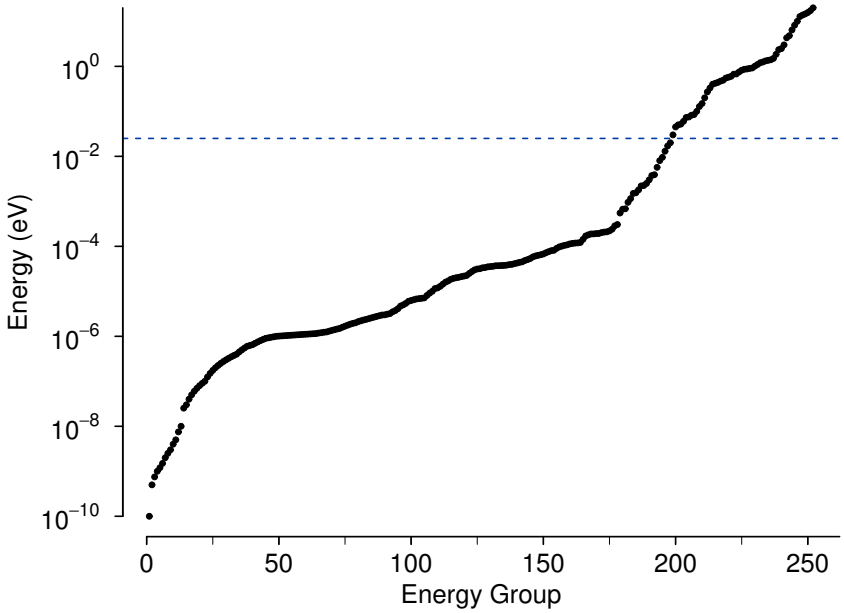

Figure 4.5: 252 energy group structure used by the JEFF-3.0/A Nuclear Data Library

accurate simulation results. The material output of the final timestep of the irradiation case was taken as the input to the first timestep of the cooldown case, again to produce the most accurate transition between the two operational states.

4.5 Radioactive Dose

The radioactive dose experienced in proximity to the MSNB was evaluated by coupling the MCNP and ORIGEN codes. The initial composition of the MSNB eutectic, as calculated by MCNP through specification of the material volumes and densities, was input in ORIGEN and subjected to a constant flux of neutrons for a number of timesteps throughout the operational period of the MSNB. Following the simulated irradiation, ORIGEN simulated a cooldown period with no neutron flux and tracked the decay of the previously produced fission products as described in Section 4.4.2. Finally, along with the total quantities of the remaining salt, fuel, and fission products produced, the code reported energy-binned and time-dependent intensities of neutrons and photons radiated from the FLiBe-UF_4 eutectic by the radioactive decay of unstable fission products. The neutron radiation intensities were output in energy bins according to the 252 group structure from JEFF-3.0/A, while the photon radiation intensities were output in 10 linearly spaced energy bins from 2 eV to 20 MeV. Alpha and beta radiation intensities were not used in the analysis, because of the limited particle fluxes that were expected to escape from the MSNB.

The ORIGEN results were then input in MCNP, with the radionuclide inventories predicted at each timestep used as the material card for the eutectic to replicate the post-operational conditions within the MSNB. The radiation intensities were used in the definition of the SDEF card to replicate the release of radiation from the eutectic. The FLiBe-UF_4 eutectic was defined as a single cell in the MCNP input

so the entire volume of the salt could easily be treated as the radiation source volume. The density of the eutectic, and the neutron data libraries used, were consistent with the material at its melting temperature. This volumetric source was defined by the CEL rejection method, in which the source cell and an enclosing volume are specified, random points are sampled within the volume, and a point is accepted as a valid source location if it is also contained within the cell. By default the sampling efficiency must be greater than 1% to prevent excessive computational time wasted on generating source points that will be rejected. Because of the large volumes not filled with the eutectic in the MSNB, particularly the reflector and the regions between the distributing spokes, the efficiency was around 20%.

Independent simulations of the neutron and photon radiation fluxes were conducted to simplify the definition of the source and the analysis of the results. Fluxes of escaping radiation at the external surfaces of the reactor were evaluated with the F2 surface flux tally within energy bins corresponding to energy-dependent flux-to-dose conversion factors. The independent contributions to the absorbed dose were then summed to produce an estimate of the total absorbed dose that would be experienced in proximity to the MSNB following shutdown.

4.6 Summary of Simulations

The following list is given to summarize the distinct simulations that were conducted to characterize the performance of the MSNB:

- Neutron flux through MSNB materials – MCNP
  - Flux through neutron reflecting materials
  - Attenuation in neutron absorbing materials
  - Moderation in molten salt
- Delayed neutron losses in dynamic systems
- Optimization of the control rod design – MCNP
  - Simulation of all combinations of control rod dimensions
- Performance of control rods through rotational range – MCNP
- Effects of removal of the control rods – MCNP
  - Replacement with air
  - Replacement with light water
  - Replacement with boron carbide
- Thermal effects on criticality – MCNP
- Characterization of neutron flux in the MSNB core – MCNP
  - Point detector arrays through height of the MSNB core
- Burnup and fission product production during operation – MCNP
  - Sequential KCODE and BURN problems (Section 4.4)
- Fission product production following operation – ORIGEN
- Estimation of radioactive dose – ORIGEN-MCNP
  - ORIGEN simulation of radiation intensities
  - MCNP simulation of flux from MSNB core

Chapter 5: Analysis and Results

5.1 Material Characterization

Results of the MCNP simulation of the most significant MSNB materials, as discussed in Section 4.1, were used to inform design decisions relating to the geometry of the core and location of the control rods. The results of the simulations of reactor grade graphite, pure beryllium metal, and BeO are shown in Figure 5.1. The results of each of the simulations were summed across the recorded energy bins and normalized to the value of the highest recorded flux to compare the relative capabilities of each material.

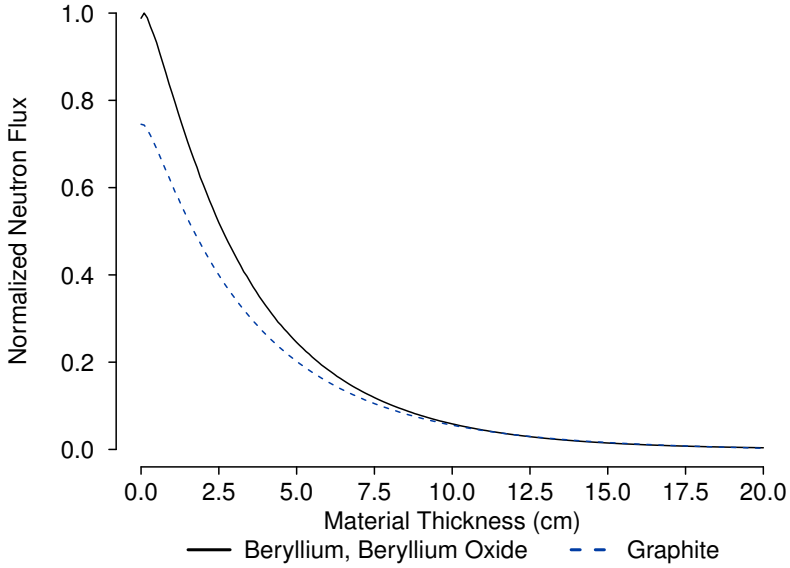

Figure 5.1: Normalized neutron fluxes through beryllium metal, BeO, and graphite

Because the measured flux at each surface in the simulation is independent of the direction of each particle passing through the surface, and simply calculated from the number of particle tracks through the surface, the tally results can be understood to be composed of both outgoing and returning neutrons. Although an initially low flux is indicative of a lower number of neutrons successfully penetrating the material to a given depth, a more valuable metric for the identification of an effective reflector is the slope of the neutron flux at a given point. A negative slope with a greater magnitude indicates that the neutron flux is changing more quickly as the thickness of the material increases. Because neutrons are ideally reflected, rather than absorbed, those which are reflected back towards the source contribute to an even higher flux at more shallow depths, further increasing the magnitude of the slope. Thus, the magnitude of the slope of the neutron flux is indicative of a greater degree of neutron reflection rather than absorption or other loss mechanisms. By this metric, beryllium and BeO were the most effective reflectors, both significantly outperforming graphite.

The results for the two beryllium-containing materials were nearly indistinguishable, differing by less than 2.0% until 9.0 cm, 5.0% until 16.0 cm, and 12.0% by 20.0 cm. These deviations are statistically

significant, with the relative error of each simulation remaining at less than 1.0% across the range of simulated thicknesses of each material. However, the slight performance gains associated with using pure beryllium were offset by other advantages provided by BeO. The density of BeO, at 3.01 $g \cdot cm^{-3}$, is 1.63 times that of beryllium metal; because the relatively light beryllium atoms contribute only 36.0% of the mass of a BeO molecule, in a given volume of each material BeO requires only 58.6% of the mass of beryllium required by pure metallic beryllium. The use of beryllium metal as the reflecting material was precluded primarily due to the anticipated availability and cost of the material, which could be nearly halved by using BeO for only slight losses in the performance of the reflector. BeO also provides a greater margin of safety with the melting temperature of the ceramic at 2507°C, almost twice that of beryllium metal. However, the thermal conductivity of BeO is nearly twice that of the metal, which could result in the transfer of heat out through the sides of the core, through the reflector, and into the cooled salt flowing downward to return to the core.

From the results depicted in Figure 5.1, it was determined that only 1.49% of all neutrons reached a depth of 20.0 cm, and fewer than 0.39% of all neutrons reached a depth of 25.0 cm. To prevent the excessive leakage of neutrons, a minimum BeO thickness of 30.0 cm was used, which reduced the neutron flux by 99.9991%. The anticipated position of the extreme outward position of the control rod plates was predicted to be between 17.0 cm and 41.0 cm depth as discussed in Sections 4.2.2 and 5.3.

The results of the neutron flux simulations for hafnium, the neutron absorber chosen for use in the neutron absorbing plates embedded in the control rods, are shown in Figure 5.2. According to the data depicted, at 0.5 cm thickness close to 42% of incident neutrons would be absorbed, leaving 58% of the incident neutrons to pass through the material.

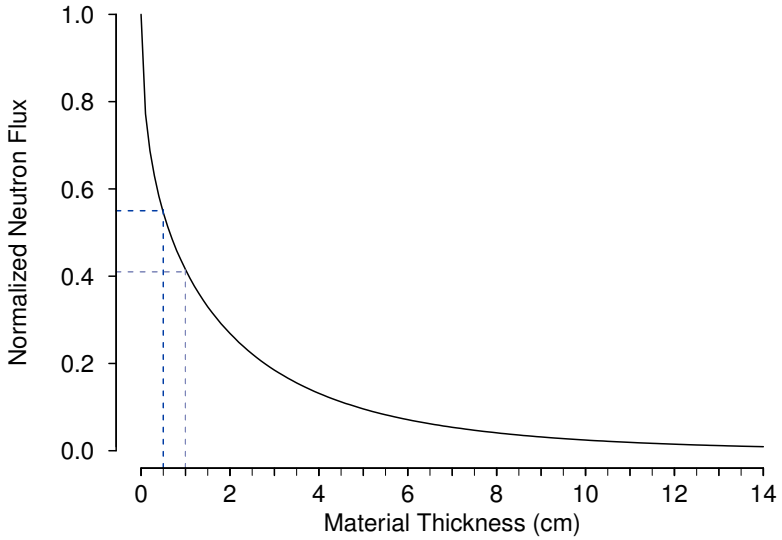

Figure 5.2: Normalized neutron flux through hafnium

Given that any neutron that passed through the hafnium unabsorbed would, in order to return to the core and contribute to the fission chain reaction, almost certainly pass back through the hafnium plate,

the thickness of the plate was effectively doubled. At 1.0 cm thickness, according to Figure 5.2, 59% of neutrons reaching the hafnium would be absorbed, with the remaining 41% returning in the direction of the core. However, this assumes that neutrons passing through the hafnium when leaving the core are instantly reflected directly back by the reflecting material in the control rod. In reality, neutrons would likely penetrate the reflecting material contained in the control rod to some depth and be reflected out in an entirely new direction. This would result in the neutron likely taking a path longer than the shortest distance through the hafnium, and a sub-optimal path back to the core. As such, it is likely that far fewer than the unabssorbed 41% of the neutrons will return to the core.

The results of the final neutron penetration simulation, conducted with the FLiBe-UF_4 eutectic, are shown in Figure 5.3. The energy-dependent tally results were divided into two energy groups: thermal neutrons below 0.025 eV and comparatively fast neutrons above 0.025 MeV. The relative populations of each group were normalized to the maximum recorded flux of each to compare changes in each population. The scale for the fast neutron flux in the figure is shown in multiples of the maximum thermal neutron flux; thus at the first surface defined in the simulation the fast neutron flux was 26 times greater than that of the thermal neutrons. However, the neutron fluxes were nearly identical at thicknesses approaching 20.0 cm.

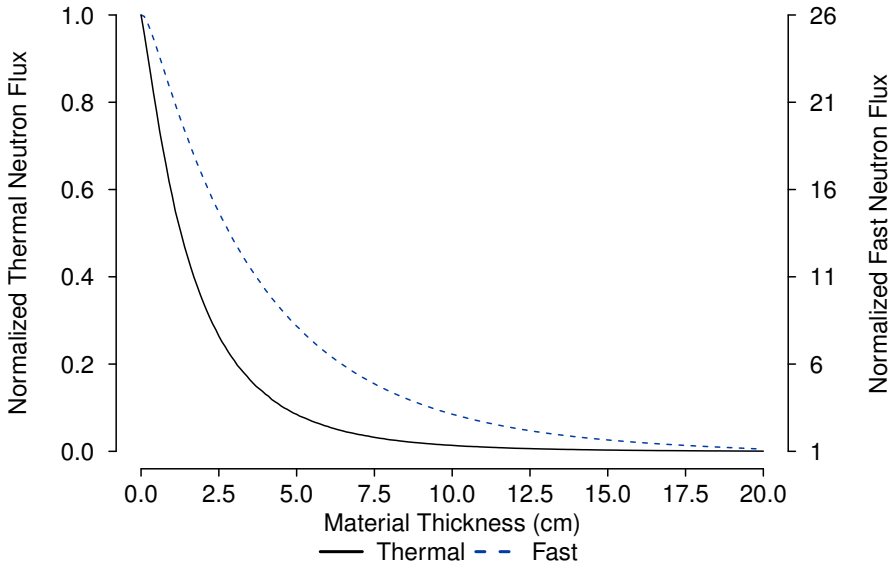

Figure 5.3: Normalized fast and thermal neutron fluxes through FLiBe

The thermal neutron population quickly fell with increasing thickness of the eutectic material, falling to less than 5% of the initial population within 10.0 cm. Because neutrons in the thermal energy range are most likely being lost in causing ^{235}U fissions, regions in the MSNB that have less than 10.0 cm of the eutectic will be inherently subcritical.

The fast neutron flux fell quickly, but not at the same rate as the thermal neutron flux. To fully utilize the entirety of the neutron energy spectrum, the data support the use of a neutron reflector and moderator. However, the energy distribution of the fission neutron spectrum is not evenly distributed

like that of the source used in this simulation, so the ratio of the populations of the thermal and fast energy groups are, in reality, expected to be different.

5.2 Delayed Neutrons

The calculated average lifetime across the delayed energy groups was 13.02 seconds for delayed neutrons in a static system, which constitute 0.65% of all neutrons created through ^{235}U fissions. After conducting the experiment to factor in the movement of the fuel through the core region in the dynamic system of the MSNB, with the given core dimensions and flow rate of the UF_4 through the core, the average lifetime was predicted to be reduced to 6.84. The reduction of the average lifetime by close to half, after accounting for the different abundances of each energy group, resulted in the reduction of the delayed neutron fraction of the entire neutron population to 0.61%. The discrepancy between the magnitudes of the changes to each characteristic is due to the the differences in the relative abundances of each delayed neutron group; groups 1 and 2, with half-lives of 55.72 and 22.72 seconds, have abundances of 3.3% and 21.9%, respectively. Group 1, in particular, represents the most frequent losses to delayed neutrons because of its relatively long half-life but low abundance.

Because the change in the delayed neutron fraction of the entire neutron population was only 0.04%, static simulations of the MSNB system in MCNP were considered to be acceptable. The uncertainties in the simulations performed by MCNP were typically in the range of 0.1% to 5% in this work, so errors due to the overestimation of the neutron population by 0.04% were deemed insignificant.

5.3 Control Rod Optimization

The results of the control rod sensitivity analysis are visualized in Figure 5.4. The largest steps in the values of the effective neutron multiplication factor resulted from increasing the distance between the control rods and the reactor core, with the earliest permutations using the closest simulated position. This parameter had the largest effect on the predicted value of the neutron multiplication factor because of the exponentially decreasing value of the neutron flux in the reflector. The control rods located at 85.00 cm, corresponding to a BeO thickness of 16.00 cm between the core and the closest point of the cylindrical control rod, were exposed to 4.47% of the incident neutron flux. The control rods located at the next closest distance, corresponding to a material thickness of 18.75 cm, were only exposed to 2.10%. On the scale of the effects introduced by the iterations of the three parameters, this is the most significant.

The next largest steps in the values of the neutron multiplication factor, within each of the steps of the control rod distance, were caused by variations in the radius of the control rods. These effects were significant for similar reasons as were changes in the control rod distance; increasing the radius of the control rod effectively moved the neutron absorbing plate closer to the core. An additional effect was the increase in the width of the neutron absorbing plates as seen from the core. Because the plates cover a larger area with an increasing control rod radius, fewer neutrons miss the control rods entirely in favor of the entire depth of the BeO reflector.

The smallest variations in the value of the neutron multiplication factor are due to changes in the thickness of the neutron absorbing hafnium plate. The variances arising from the plate thicknesses are

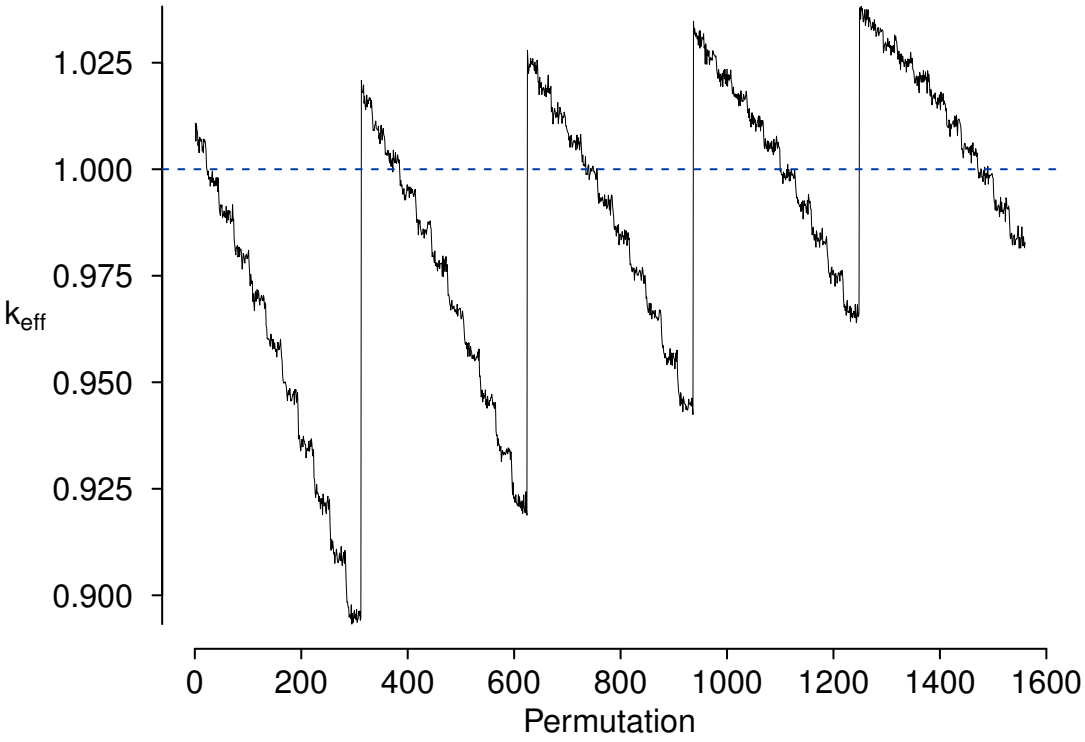

Figure 5.4: Results of control rod optimization sensitivity analysis

within the standard deviations reported by MCNP. It can be understood that even at the minimum distance used in the control rod optimization, so few neutrons reached the control rods that even the smallest absorber thickness tested was sufficient for complete capture of those neutrons.

The most optimal control rod design satisfied the criteria described in Section 4.2.2; the design must have the largest control rod radius, be located the farthest from the MSNB core, have the thinnest possible neutron absorber plate, and be able to bring the neutron multiplication factor below unity with the control rods rotated inward. The design satisfying the first, second, and fourth criteria was chosen according to the results depicted in Figure 5.4. The choice of the neutron absorbing thickness could not be made based on this data, because of the magnitude of the variation of the neutron multiplication factor between simulations. The design decision was informed by the data visualized in Figure 5.2, with the desired thickness reducing the neutron flux approximately by half. The final combination of control rod design parameters is given in Table 5.1.

Following the selection of the final control rod design parameters, the chosen design was evaluated through the full range of its rotational positions. The value of the MCNP-calculated effective neutron multiplication factor as a function of the control rod position is shown in Figure 5.5. The fully rotated inward position, at 0° in the figure, is depicted in Figures 4.3 and 4.4; the center of each neutron absorbing plate lies directly between the centers of its control rod and the MSNB core. Because of the location of the hafnium absorber in its closest proximity to the core and the simultaneous occlusion of the BeO reflector

Parameter	Value (cm)
Distance, Center to Center	91.75
Radius	12.50
Neutron Absorber Plate Thickness	0.50

Table 5.1: Final control rod design parameters

contained in the control rods, the neutron multiplication factor of the system is at a minimum when the control rods are in this position. The fully rotated outward position, at 180° in Figure 5.5, has the neutron absorbing plate located on the opposite side of the control rod. With the greatest volume of neutron-reflecting BeO between the core and the hafnium absorber in this position, the neutron multiplication factor of the system is at its highest when the control rods are in this position. At intermediate positions the hafnium plate is located at a point along the circumference of the control rod, between the two extreme positions. The neutron multiplication factor between the extreme positions can be determined by a simple trigonometric function, as shown in Figure 5.5. Thus, the greatest change in the neutron multiplication factor per unit rotation is achieved when the control rod is in the 90° position.

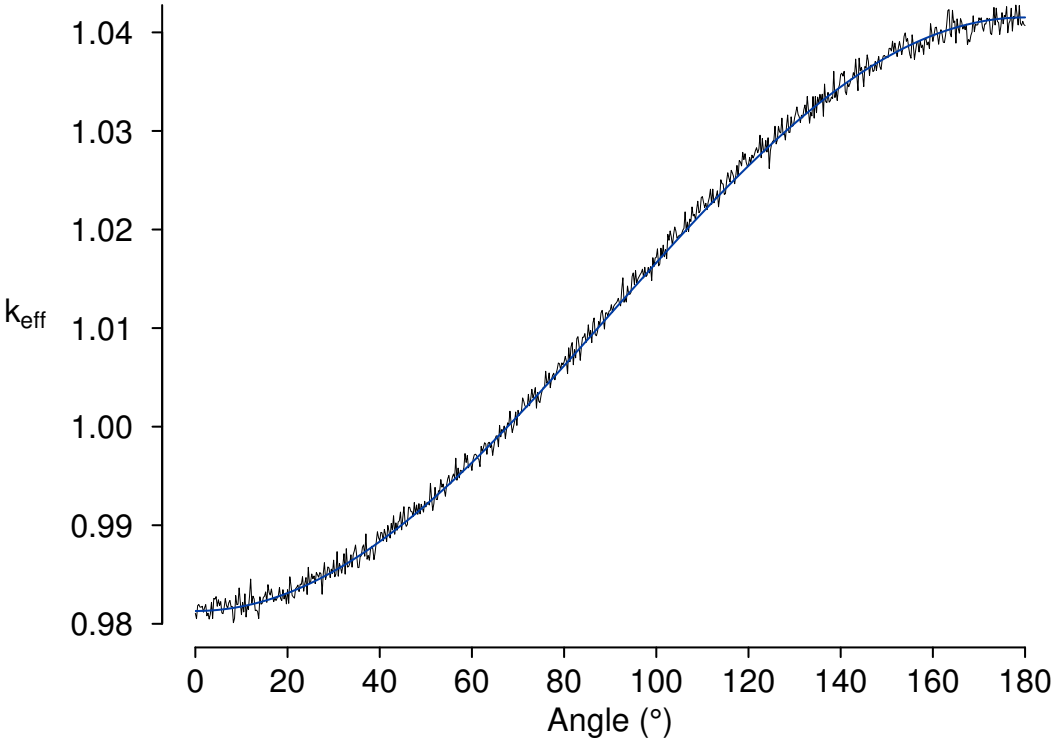

Figure 5.5: Predicted effective neutron multiplication factor across the range of rotational control rod positions

MCNP predicted a neutron multiplication factor of 1.01956 ± 0.00073 for the system when the control rods were removed and replaced with an equivalent volume of air, as could occur during transport of the MSNB or an accident scenario. The optimization of the control rod design parameters had a significant effect on the results of this simulation, as the radius of each control rod determines the size of the air gap, while the position of the control rods simultaneously changes the location of the gap. Given these results, additional safety measures would have to be taken to render the system subcritical in any event that involves the removal of the control rod. Such measures would likely consist of the insertion of solid neutron poisons into the gaps to remove as many neutrons as possible from the system. Measures should also be taken to seal the gaps if the control rods are not inserted; filling the gaps with water, which could conceivably enter the system and serve to more effectively moderate the fission neutrons, results in an effective neutron multiplication factor of 1.01026 ± 0.00085.

A final series of simulations were conducted with the candidate material boron carbide. Boron, particularly its isotope ^{10}B, has a large neutron cross section and is commonly used in the control of nuclear reactor criticality. The result of filling each of the MSNB control rod channels with the material was an effective neutron multiplication factor of 0.97724 ± 0.00082, demonstrating that boron carbide is an effective candidate for maintaining the system in a subcritical state. Lastly, a simulation with a pair of opposing control rods replaced with air and the remaining channels filled with boron carbide was conducted. Such a situation would occur during the transition from boron carbide to the control rods to be used in operation. The results indicate that even with only six channels filled with boron carbide the system remains subcritical, with an effective neutron multiplication factor of 0.98835 ± 0.00084.

5.4 Thermal Effects

The results of the MCNP simulation of the system criticality for core inlet temperatures ranging between 600°C and 1200°C are shown in Figure 5.6. In this temperature range, the relationship between temperature and the neutron multiplication factor is linear, with a marked decrease in the neutron multiplication factor with increasing temperature. In an accident scenario in which the FLiBe-UF_4 eutectic rises above its nominal temperature, a strong negative temperature reactivity feedback effect is expected to render the system subcritical and allow the temperature to return to steady state levels.

5.5 MSNB Core Neutron Flux

The results of MCNP simulations are almost always normalized by a set particle weight. In most problems, each particle has unit weight, so that the tally results are given per source particle. In MCNP KCODE problems that are run only to determine the value of the effective multiplication factor, no manipulation of the data is required to extract meaningful data from the simulation output. However, in KCODE problems where the developed criticality source is used as a particle source to be measured by other tallies, tallies are normalized differently, and the tally results must be treated to provide useful data. Following the methods described by Žerovnik, Podvratnik, and Snoj, the Equation 5.1 equation was used to normalize the neutron flux tallies measured from a KCODE source [19].

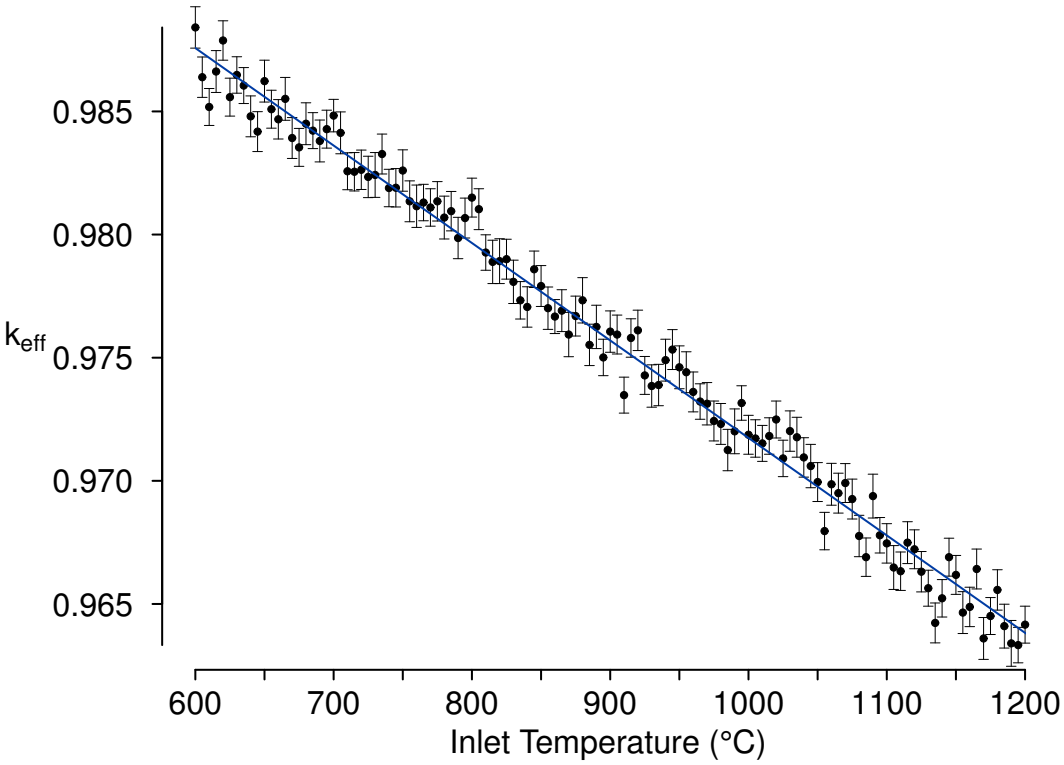

Figure 5.6: Correlation between MSNB inlet temperature and predicted effective neutron multiplication factor

$$C = \frac{P\langle\nu\rangle}{\langle w_f\rangle k_{eff}} \tag{5.1}$$

where C is the scaling factor to be applied to the tally results, P is the reactor thermal power, $\langle\nu\rangle$ is the average number of neutrons produced per fission, $\langle w_f\rangle$ is the average energy released per fission event, and k_{eff} is the effective neutron multiplication factor.

The MCNP simulations of flux in the MSNB core produced an output file for each radial layer simulated. Each of the output files contained data corresponding to each of the 100 point detectors and included cartesian coordinates, the total tallied flux, and the uncertainty of the tally. Because the point detectors in each simulation filled a wedged-shaped region spanning one eighth of the reactor, a large part of the analysis involved manipulating the data to span the entirety of the core. The point detector data from each of the output files was extracted and concatenated into a single list of data. Iterating through the data by height within the core, the data in each layer were inserted into a matrix according to their coordinates. The matrix was then mirrored and concatenated with itself horizontally and vertically, and then concatenated with its own transpose to form a complete image of the neutron flux in each radial layer. Because each completed matrix was stored in a list of matrices, various flux profiles across the MSNB core could be investigated by programmatically extracting the data. Determining the radial flux

at any height within the core required only accessing the appropriate matrix. Determining the axial flux required accessing the appropriate sequences of matrix elements within each matrix in the list, such as every element in the central row of each matrix to return the axial flux in the plane of the x-axis.

Visualizations of the radial neutron flux at several heights above the bottom of the MSNB core are presented in Figure 5.7. The neutron fluxes at 0.01 cm and 134.11 cm are at positions 0.01 cm above and below the bottom and top of the core, respectively. The 8.95 cm and 125.17 cm positions are located two point detector steps, 4.47 cm each, from the upper and lower extreme positions. The radial flux at 67.06 cm height is the closest to mid-height within the core.

Several effects can be noted at the heights of each of the radial fluxes. Most prominent are the dampening effects of the neutron absorbing plates arranged in 45° increments, starting at 22.5° from the positive x-axis. Along lines extending radially in each of these directions the neutron flux is typically at a local minimum; this effect is most easily seen at the 125.17 cm height because of the relatively thin layer of BeO reflector located above the core, which in other locations has the effect of homogenizing the neutron flux. The maximum neutron flux at each height typically occurs in a ring around the centerline, rather than in a point on the centerline. This is most likely due to the significant reliance on the BeO reflector for the system to achieve criticality, which has the effect of offsetting the point of maximum flux radially towards the reflector. At the extreme upper and lower edges of the core, lower fluxes can be observed in a ring around 25.0 cm radius, corresponding to the zircalloy barrier in the risers between the FLiBe-UF_4 eutectic and the BeO reflector. At the bottom of the core, lower fluxes can be observed on radial lines starting at 45° from the positive x-axis, and then every 45° after. These regions correspond to the eight spokes returning the eutectic to the lower riser. Although the presence of the eutectic could contribute to higher fluxes along these lines, each spoke is surrounded by stainless steel, which blocks a large fraction of the neutron flux escaping from the spokes. Additionally, in the lower region of the reactor the spokes pass through the reflector; the loss of the BeO reflecting material along these lines contributes to the low flux.

The axial neutron flux in two planes is shown in Figure 5.8. The first plane, at 0° and along the x-axis, shows the neutron flux in a plane passing between sets of control rods. The second plane, at 22.5° from the positive x-axis, shows the neutron flux in a plane passing through the centers of control rods located on opposite sides of the MSNB core.

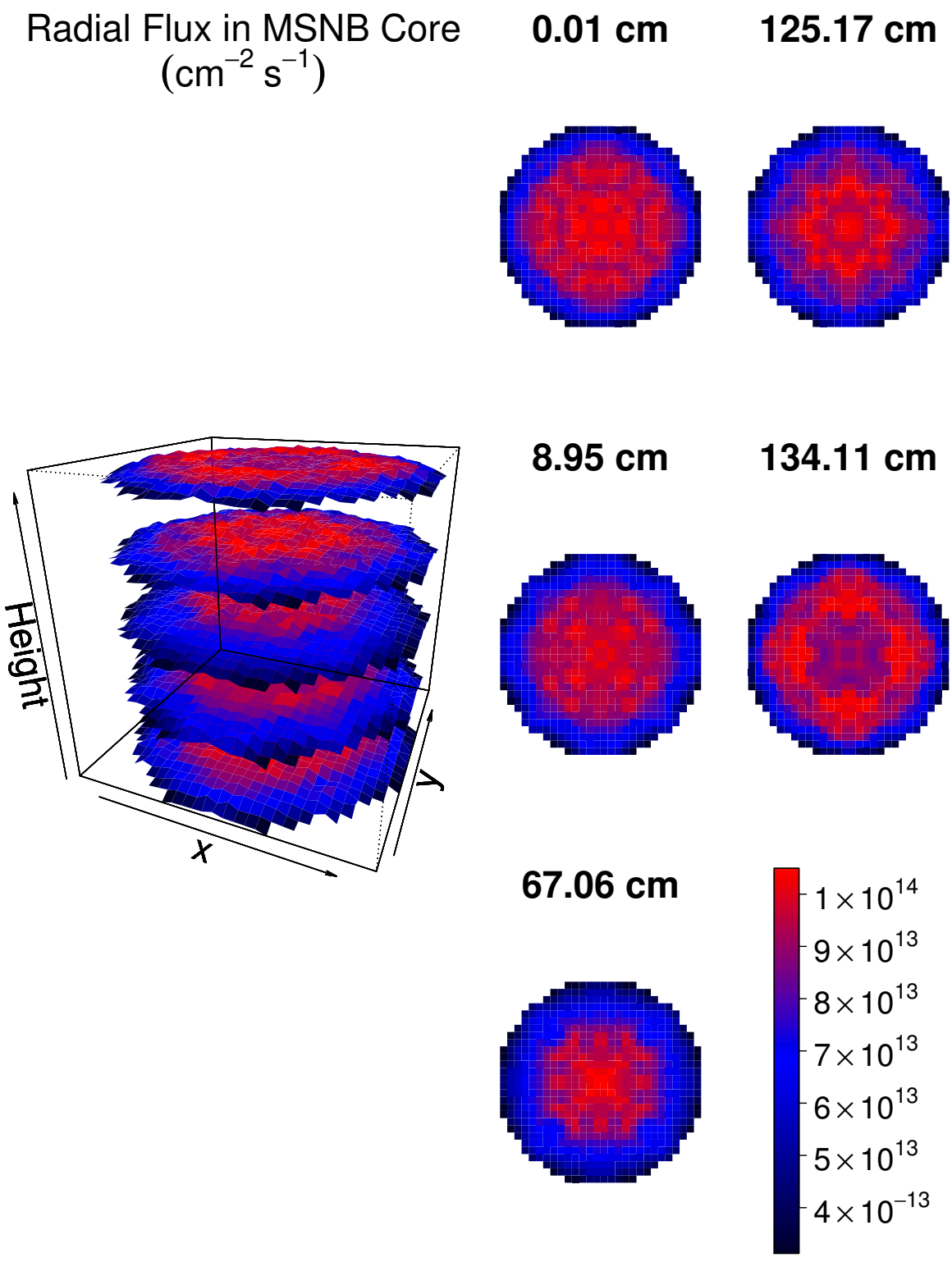

Figure 5.7: Normalized radial neutron flux at select heights in the MSNB core

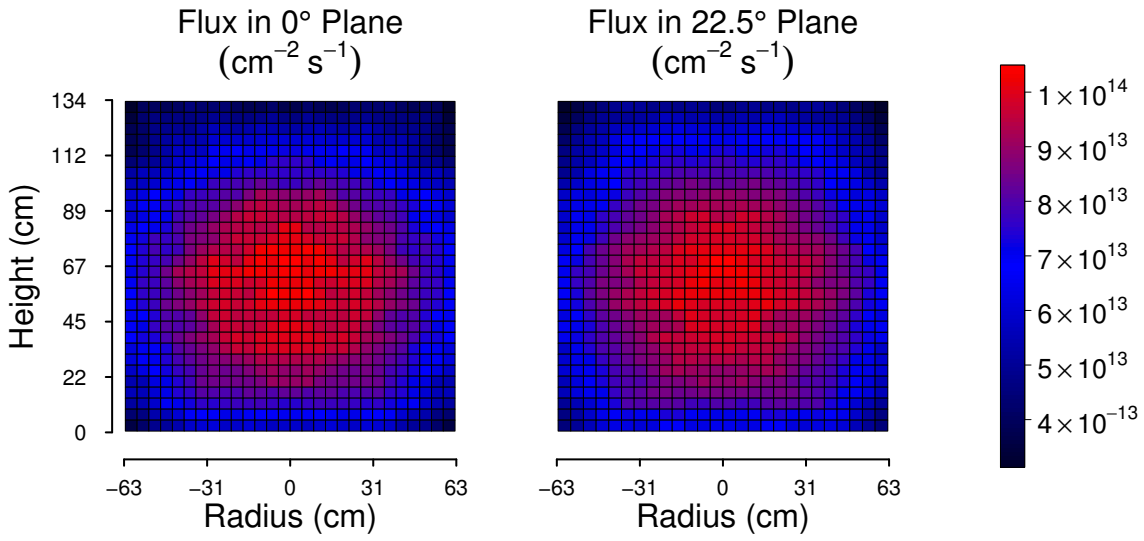

Figure 5.8: Normalized axial neutron flux in select planes in the MSNB core

It can be seen that the neutron flux is homogeneous across the height of the core, with a maximum near the center that decreases in all directions towards the fringes of the core. The location of the maximum is shifted below the midpoint of the core, due to the larger volume of BeO reflector located below the core than above. In the plane of the control rods, the axial flux decreases more quickly than in planes that do not pass through the control rods. The effects of the control rods on the axial neutron flux can be more clearly seen in Figure 5.9, which plots the radial fluxes at various heights along each of the two planes of Figure 5.8.

Near the top and the bottom of the core, the close proximity of the BeO reflector near the centerline of the core results in the homogenization of the neutron fluxes in both planes. This is due to the predominant effects of the reflector in the regions that are relatively far and well-insulated by the intervening from the control rods. Near the edges of the core, however, the effects of the control rods become more prominent, and the neutron flux in the plane aligned with the control rods falls more quickly. Near the mid-height of the core, the predominant effect on the level of the neutron flux is the control rods, because of the relatively large distance between the upper and lower reflector. At this point, the neutron flux in the plane of the control rods begins to fall below that of the other plane much sooner, and the two axial fluxes are not as identical near the reactor centerline.

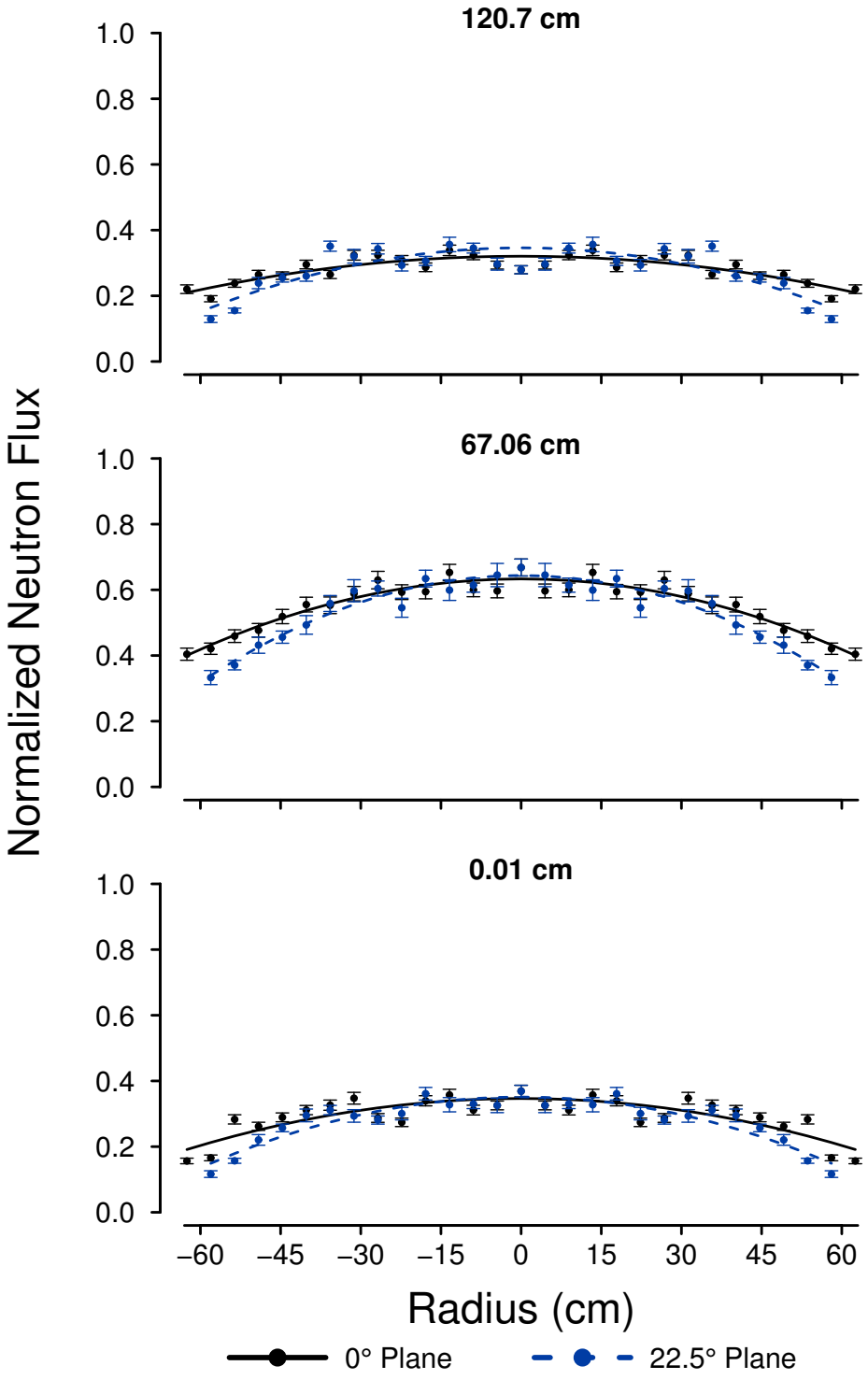

Figure 5.9: Comparison of neutron fluxes in the MSNB core, at select heights and in select planes

5.6 Operation and Burnup

Following the completion of the successive simulations of the full MCNP operational period, the initial analysis involved extracting the final calculated effective neutron multiplication value and control rod position information from the output files associated with each complete timestep. This data is shown in Figure 5.10 for a series of simulations using the second tier of fission products, a 7% UF_4 fuel loading, and 10-day timesteps.

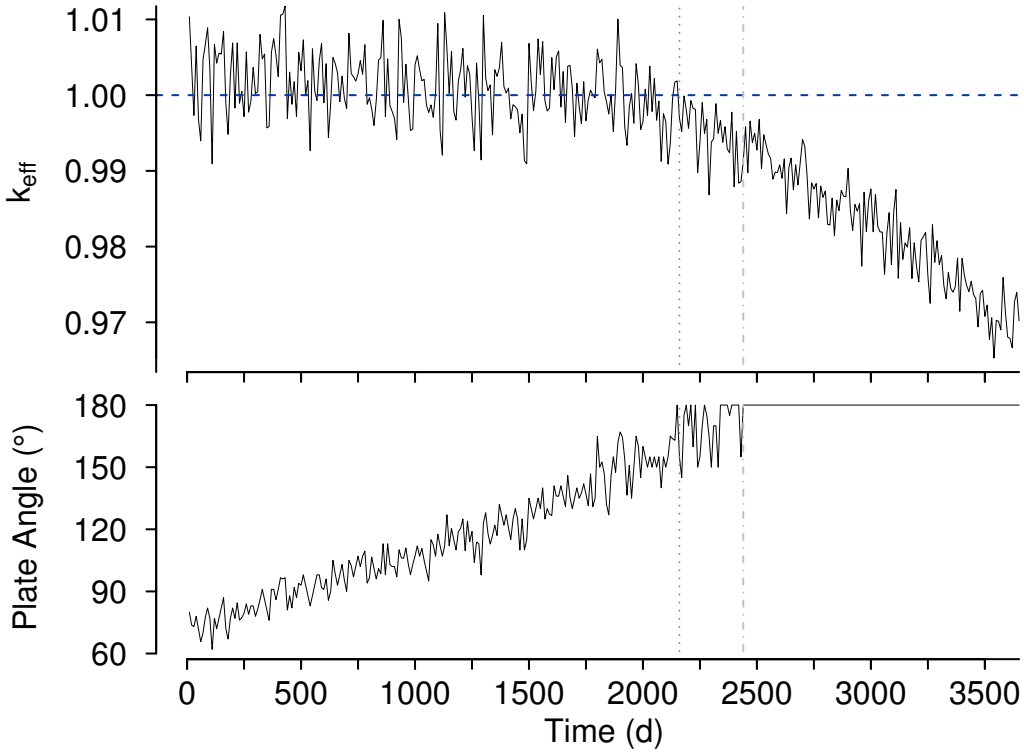

Figure 5.10: MSNB performance over 10 years with Tier 2 MCNP fission products

The performance of a particular initial configuration of the MSNB was determined on the basis of: the length of the operational period completed; the value of the effective neutron multiplication factor through subsequent timesteps; and the average burnup achieved during operation, calculated as the difference in the mass of ^{235}U present before and after operation.

The first vertical line in Figure 5.10 indicates the last point in time at which the value of the neutron multiplication factor was greater than unity, following which the value steadily declined until the end of the simulated time period. The second vertical line indicates the point at which the control rods reached the fully rotated outward position and stayed for the remainder of the simulated time. The MSNB with this initial configuration reached 2150 days, or 5.89 years, of continuous critical operation at 10 MWth before reaching a nonrecoverable subcritical configuration. Given an initial ^{235}U mass of 360.6 kg and a final mass of 297.0 kg, the MSNB consumed 63.6 kg of ^{235}U and achieved a burnup of 17.6%.

There are several competing effects that arose through this method of simulating the operation of the MSNB that introduced uncertainty into the results. The most significant are the size of the simulation timesteps, management of the buildup of the neutron poison ^{135}Xe, and uneven burnup of the ^{235}U fuel. It was theorized that the excessive buildup of ^{135}Xe was the most significant of these effects; another operational simulation was conducted that excluded ^{135}Xe from the transport calculation, the results of which are shown in Figure 5.11.

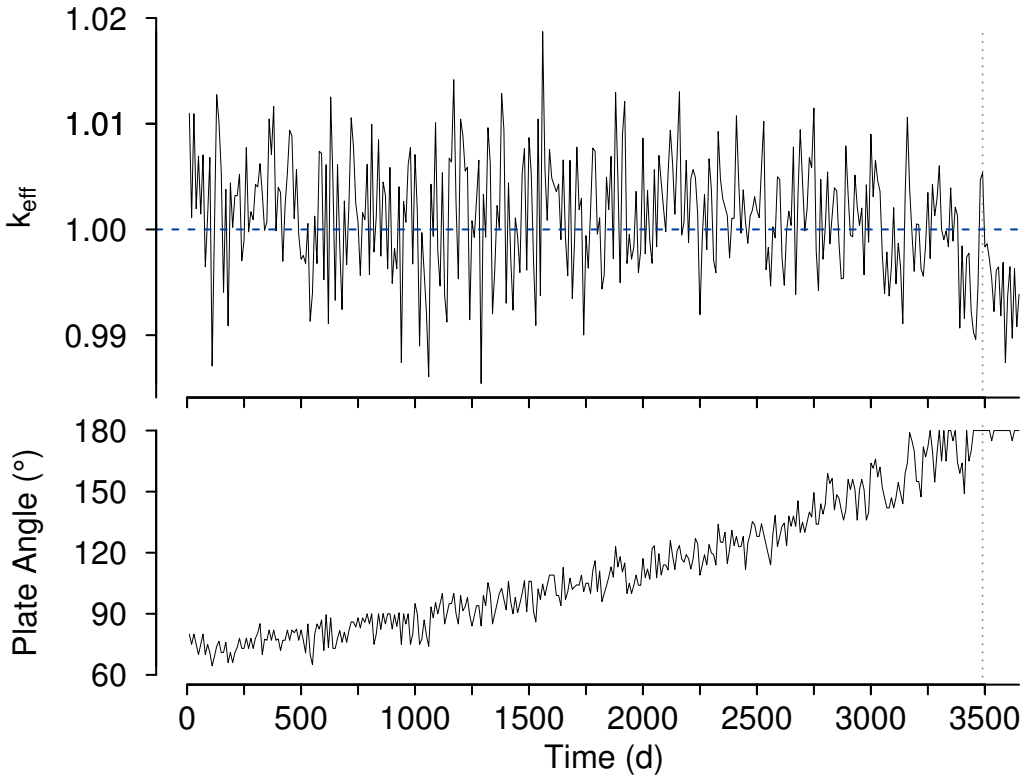

Figure 5.11: MSNB performance over 10 years with no ^{135}Xe transport

The vertical line in Figure 5.11 indicates the last point at which the simulated MSNB had a neutron multiplication factor greater than unity, occurring at 3490 days, or 9.56 years. The burnup in this simulation was identical to that of the preceding simulation, with identical masses of ^{235}U present at the start and end of each. The 62% increase in the achievable operational period between the two preceding cases is due solely to omission of ^{135}Xe from the MCNP transport calculation. This result lends support to the hypothesis that the excessive buildup of the isotope is one of the most significant detriments to the operational period achievable by the MSNB.

5.6.1 Xenon-135 Buildup

The radionuclide ^{135}Xe is the most significant known neutron poison, with a neutron absorption cross section around 2,650,000 barns [20]. Some ^{135}Xe is produced within a nuclear reactor directly as a fission product, but the majority comes from the radioactive decay of its parent fission products ^{135}Te and ^{135}I

as follows [21]:

$$^{135}\mathrm{Te} \xrightarrow[19.0\,\mathrm{s}]{\beta^-} {}^{135}\mathrm{I} \xrightarrow[6.58\,\mathrm{h}]{\beta^-} {}^{135}\mathrm{Xe}$$

^{135}Xe equilibrium in a system is achieved when the production of the radionuclide is balanced by its loss. The built up ^{135}Xe is lost either through neutron capture, becoming the effectively stable isotope ^{136}Xe, or through beta decay to ^{135}Cs with a 9.14 hr half life [21]. The balance of ^{135}Xe contained in the system can be calculated according to the differential equations:

$$\begin{aligned} \frac{\partial N_\mathrm{I}}{\partial t} &= \gamma_\mathrm{I}\Sigma_f\phi - \lambda_\mathrm{I}N_\mathrm{I} \\ \frac{\partial N_\mathrm{Xe}}{\partial t} &= \gamma_\mathrm{Xe}\Sigma_f\phi + \lambda_\mathrm{I}N_\mathrm{I} - \lambda_\mathrm{Xe}N_\mathrm{Xe} - \sigma_\mathrm{Xe}N_\mathrm{Xe}\phi \end{aligned} \tag{5.2}$$

where N is the concentration of the given radionuclide, t is time, γ is the fission yield, Σ_f is the macroscopic fission cross section of ^{235}U, ϕ is the neutron flux, λ is the radionuclide decay constant, and σ_{textXe} is the microscopic absorption cross section of ^{135}Xe. Although ^{135}Te is the radionuclide in the ^{135}Xe decay chain with the highest fission yield, its 19.0 s half life is short enough that its fission yield can simply be added to that of ^{135}I, which has a half life of 6.58 hr [21]. Because the half life of ^{135}I is less than the 9.14 hr half life of ^{135}Xe, ^{135}I will reach equilibrium before ^{135}Xe. In this case the rate of decay of ^{135}I, and its contribution to the production of ^{135}Xe, is equal to the rate of its production. As a result, the fission yield of ^{135}Xe can be expressed as the sum of those of each of the three radionuclides. Setting $\frac{\partial N}{\partial t} = 0$ and solving Equation 5.2 for N yields the equilibrium concentrations for ^{135}I and ^{135}Xe:

$$\begin{aligned} N_{\mathrm{I},\infty} &= \frac{\gamma_\mathrm{I}\Sigma_f\phi}{\lambda_\mathrm{I}} \\ N_{\mathrm{Xe},\infty} &= \frac{\gamma_\mathrm{Xe}\Sigma_f\phi + \lambda_\mathrm{I}N_\mathrm{I}}{\lambda_\mathrm{Xe} + \sigma_\mathrm{Xe}\phi} = \frac{\gamma_\mathrm{Xe} + \gamma_\mathrm{I} + \gamma_\mathrm{Te}}{\lambda_\mathrm{Xe} + \sigma_\mathrm{Xe}\phi}\Sigma_f\phi \end{aligned} \tag{5.3}$$

Following an increase in reactor power level, as would occur during startup, the quantity of ^{135}I in the system immediately begins to increase to its equilibrium value, which is proportional to the reactor power. Because close to 94% of ^{135}Xe is produced as the result of ^{135}I decay, the rate of the increase of ^{135}Xe towards its equilibrium value is dominated by the half life of its parent radionuclide. Thus, ^{135}Xe typically reaches its equilibrium value in 40 to 50 hours, corresponding to roughly 6 to 8 ^{135}I half lives [22]. Assuming that the MSNB operates under full power conditions for the remainder of its operational period following startup, ^{135}Xe concentrations should remain at their equilibrium value for the entirety of MSNB operation.

However, as discussed in Section 2.1.2, once the concentration of xenon reaches its saturation point in the FLiBe-UF_4 eutectic, the gas will begin escaping from the solution. In reality the equilibrium concentration of xenon is determined by its saturation point in the eutectic and not the neutron flux of the reactor, apart from the exceptional case of operation at very low levels of neutron flux. It is this action that contributes to the inaccuracy of the MCNP operation and burnup simulations. MCNP cannot account for the saturation point of the gas in the eutectic, and will allow the buildup of ^{135}Xe until it reaches its equilibrium concentration as determined by the neutron flux.

The excessive buildup of the neutron poison is especially detrimental to the results of the simulations

because of the means by which MCNP determines the criticality of the system; that is, by balancing Equation 3.5. When a reactor enters a subcritical state, the neutron flux begins to fall rapidly and the fission chain reaction ceases. In an MCNP-simulated system, however, the neutron flux at criticality and just below it are nearly identical, because the code is only trying to balance the eigenvalue equation. As a result, the neutron economy of the simulated MSNB is severely reduced with the buildup of excessive ^{135}Xe, and unnecessary ^{235}U is burned.

The concentration of ^{135}Xe in the simulated system can be managed, but only between burnup timesteps. With timesteps any longer than the time required for the concentration of xenon gas to build to its saturation point in the eutectic, excess ^{135}Xe will be built into the system. However, even with timesteps on the scale of the xenon buildup time, exact management of the concentration of the poison is unachievable. The problem is depicted in Figure 5.12, which qualitatively shows the buildup of ^{135}Xe to the saturation point of the gas in reality, the buildup and complete elimination of the isotope in the MCNP model with ten day timesteps, and an attempt to more realistically manage the concentration of the isotope with a shorter simulation timestep.

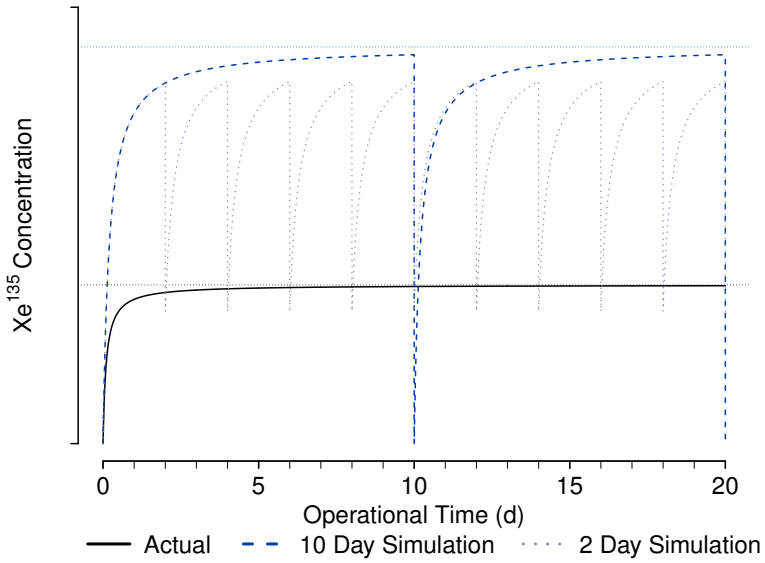

Figure 5.12: Depiction of ^{135}Xe buildup in the MSNB core in realistic operations and in MCNP simulations

With a shorter timestep, the issue becomes one of choosing a concentration value to which the ^{135}Xe should be reset between each timestep. The concentration can be set to the expected concentration of the real system, but it will immediately build beyond the realistic concentration after beginning the next timestep. Choosing a value low enough will allow the concentration to build to the correct value by the end of the timestep, but the simulated concentration will remain too low throughout the remainder of the timestep. Without continual management of the concentration of ^{135}Xe in the MSNB system, inaccuracies will begin to develop.

5.6.2 Uranium-235 Burnup

Although the analysis conducted in Section 5.2 determined that the flow of the fuel through the core only resulted in a loss of 0.04% of the total neutron population, deficiencies in the capabilities of MCNP begin to arise in the simulation of the MSNB over longer periods of time. In the real system, as the eutectic flows through the core and the fissile isotopes begin to fission, the mixture becomes slightly depleted in UF_4. Because the fuel is suspended in the eutectic mixture, though, as it circulates throughout the system the mixture will homogenize and distribute the remaining fuel. However, the MCNP simulation of the reactor treats it as a static system through each timestep. The fuel can be redistributed between each timestep by summing the burnup results and dividing them equally between each of the eutectic-containing cells, but during each timestep an excessive degree of burnup is achieved in the core region, while the remaining fuel remains mostly unburned.

Because MCNP treats the model as a static system, other effects arising from the flow of the eutectic throughout the system are not recreated. One of the most significant omissions is the flow of the eutectic through the core. A Computational Fluid Dynamics (CFD) model of the MSNB core, shown in Figure 5.13, shows that small vortices develop in the corners of the core. As a result, less fluid mixing and a greater degree of burnup will be achieved in these regions, effectively changing the critical configuration of the core over time. The periodic perfect homogenization of the eutectic utilized in the MCNP simulation does not account for this effect.

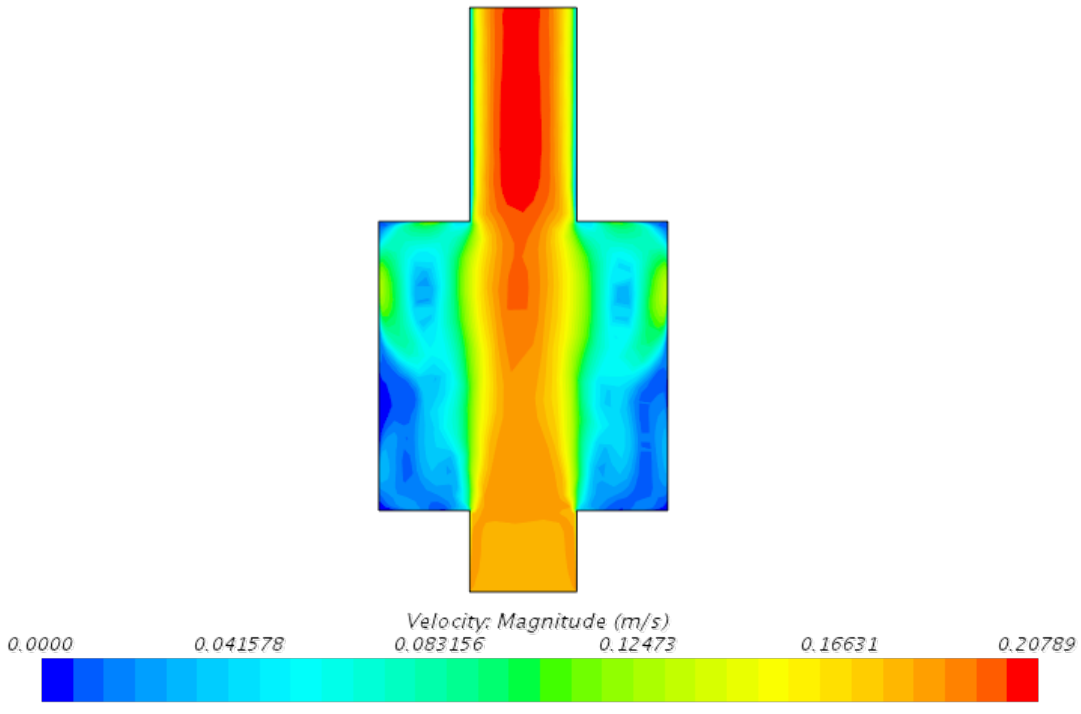

Figure 5.13: CFD model of fluid flow within the MSNB core

5.7 Fission Product Production

The results of the ORIGEN simulations included hundreds of nuclides, grouped by their masses and activities across all of the simulated timesteps. Among the fission and decay products built up in the system, several radionuclides of interest include short-lived and medium-lived fission products, which are responsible for the bulk of the radioactivity emitted from the reactor over their respective time periods. The most active short-lived fission products, which dominate the the emission of radiation over the first two to three years, were reported by ORIGEN as ^{144}Ce and ^{144}Pr, ^{106}Ru and ^{106}Rh, and ^{147}Pm. After three years the medium-lived fission products, with half lives around 30 years, constitute the bulk of the emitted radiation. The major constituents of this group are ^{137}Cs and ^{90}Sr. Figure 5.14 shows the relative activities of each of these groups of radionuclides during and after the operational period of the MSNB.

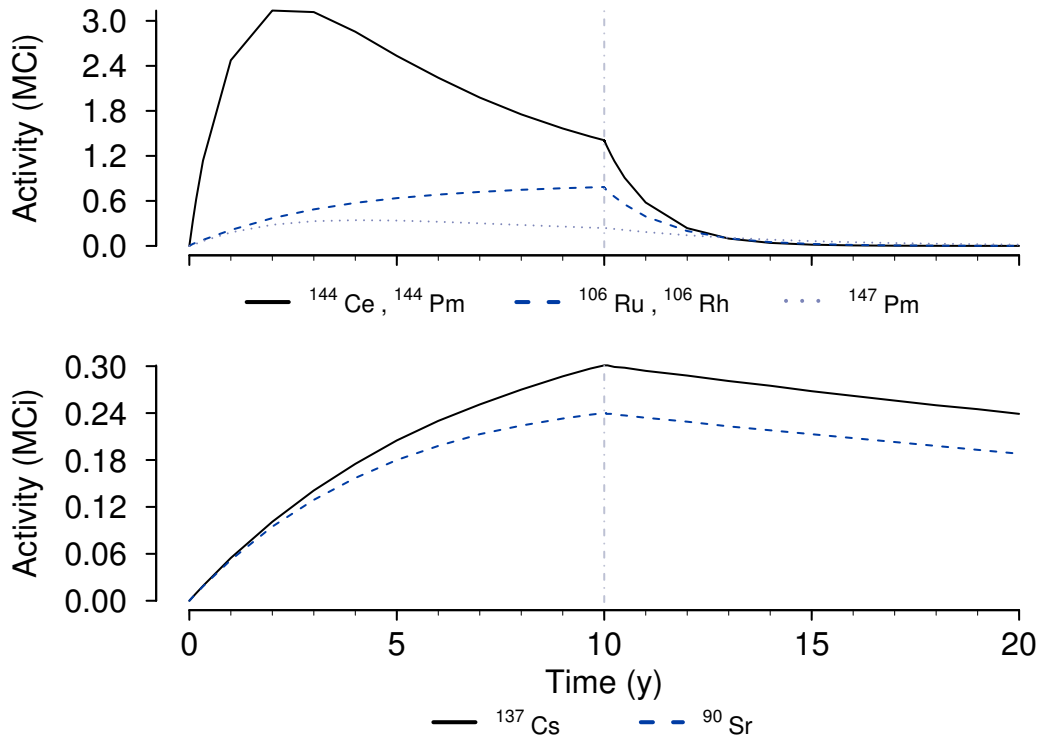

Figure 5.14: Activities of short-lived and medium-lived fission products during and after MSNB operation

Due to the presence of the beryllium isotope ^{9}Be, the MSNB FLiBe-UF_4 eutectic is also expected to produce significant quantities of tritium through the following three step reaction, which is initiated by a low energy neutron [23]:

$$^{9}_{4}\mathrm{Be} \xrightarrow{(\mathrm{n},\alpha)} {}^{6}_{2}\mathrm{He} \xrightarrow[0.81\,\mathrm{s}]{\beta^-} {}^{6}_{3}\mathrm{Li} \xrightarrow{(\mathrm{n},\alpha)} {}^{3}_{1}\mathrm{H}$$

Small quantities of tritium are also infrequently produced directly from the fissioning of ^{235}U. The

ORIGEN-calculated activity of the built up tritium is shown in Figure 5.15:

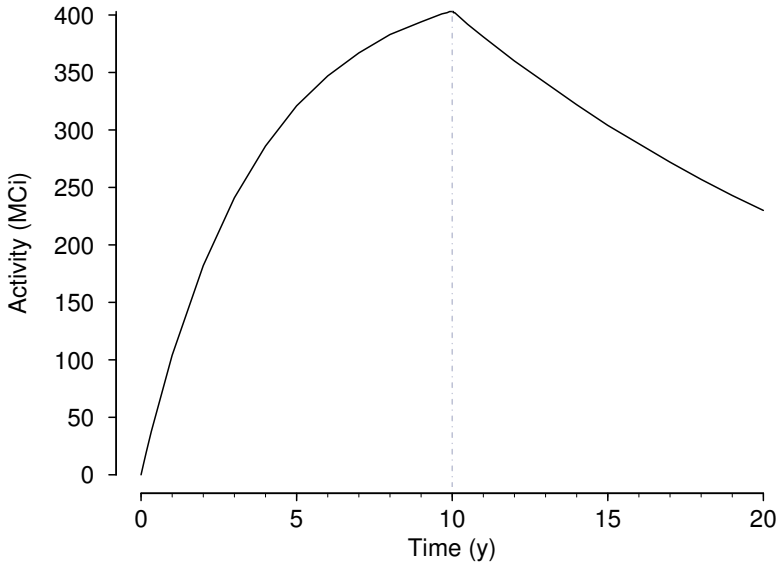

Figure 5.15: Activity of produced tritium during and after MSNB operation

5.8 Radioactive Dose

The ORIGEN-calculated total photon intensities at each timestep were used as the scaling factors to convert the MCNP surface flux tally results to real photon fluxes. The neutron flux tally results were converted to real neutron fluxes by applying Equation 5.1 to determine the neutron production rates in the cooling MSNB core. The thermal power of the reactor to be used in the calculation of the neutron scaling factor, the main source of which is the decay of radioactive fission products, was calculated according to the equation given by Todreas and Kazimi [24]:

$$P = P_0 \; 0.066 \left(t_s^{-0.2} - (t_s + \tau_s)^{-0.2} \right) \tag{5.4}$$

where P is the thermal power at a time t_s, P_0 is the operational thermal power of the reator, t_s is the time elapsed since reactor shutdown, and τ_s is the length of time the reactor operated prior to shutdown.

After converting the MCNP results to actual particle fluxes, the energy binned fluxes of each particle at each post-operation timestep were converted to absorbed dose by means of conversion factors supplied by the International Commission on Radiological Protection [25] and the United States Nuclear Regulatory Commission [26]. To then calculate the dose equivalent, the absorbed dose was multiplied by the appropriate quality factors. These data are shown in Tables A.1 and A.2 in Appendix A.

The equivalent dose was summed for both neutron and photon radioactive doses in two configurations: the unshielded MSNB in air and in a proposed cask design. The results of the simulated flux escaping the reactor, converted to dose equivalent, are presented in Figures 5.16 and 5.17. In the first case, the dose was evaluated next to a reactor without any radiation shielding beyond the inherent self-shielding

of the MSNB materials. In the second case, the cask was placed inside a proposed transportation cask design composed primarily of steel and concrete.

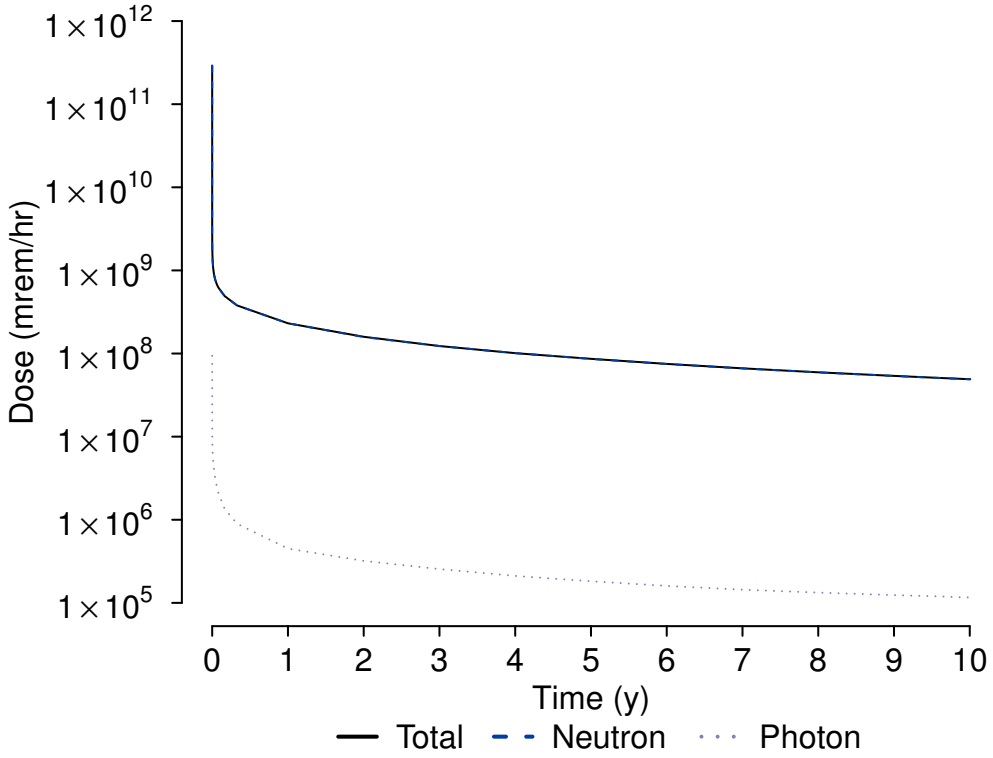

Figure 5.16: Predicted dose for the unshielded MSNB following operation

The calculated equivalent dose experienced in proximity to the MSNB following operation quickly decreases immediately after shutdown as the most short-lived radionuclides decay. Within one day, the equivalent dose falls from $2.91 \cdot 10^{11}$ mrem/hr to $1.60 \cdot 10^{9}$ mrem/hr; by 60 days the total dose is $4.91 \cdot 10^{8}$ mrem/hr, after which time the rate of decline is significantly reduced. At the end of the 10 year cooldown period the equivalent dose is predicted to fall by another order of magnitude to $4.91 \cdot 10^{7}$ mrem/hr.

The proposed cask design was effective in eliminating the flux of low energy photons and reducing the flux of some intermediate energy photons. However, due to the less significant contribution of lower energy photon radiation to the total photon dose, the photon contribution to the combined dose is reduced by less than 0.20%. The cask was more effective in attenuating the neutron dose contribution, particularly in the intermediate energy range, resulting in a reduction of 9.05% across the entire cooldown period. Because neutron radiation is the main contributor to the combined dose, the inclusion of the cask effectively reduces the total equivalent dose experienced in proximity to the MSNB by approximately 9% at each timestep over the ten year cooldown period.

It is intended that, following the completion of the operational period, the entire MSNB system is transported away from the installation site for the processing and eventual disposal of the contaminated materials. United States Regulatory Commission regulations set the following standards for acceptable

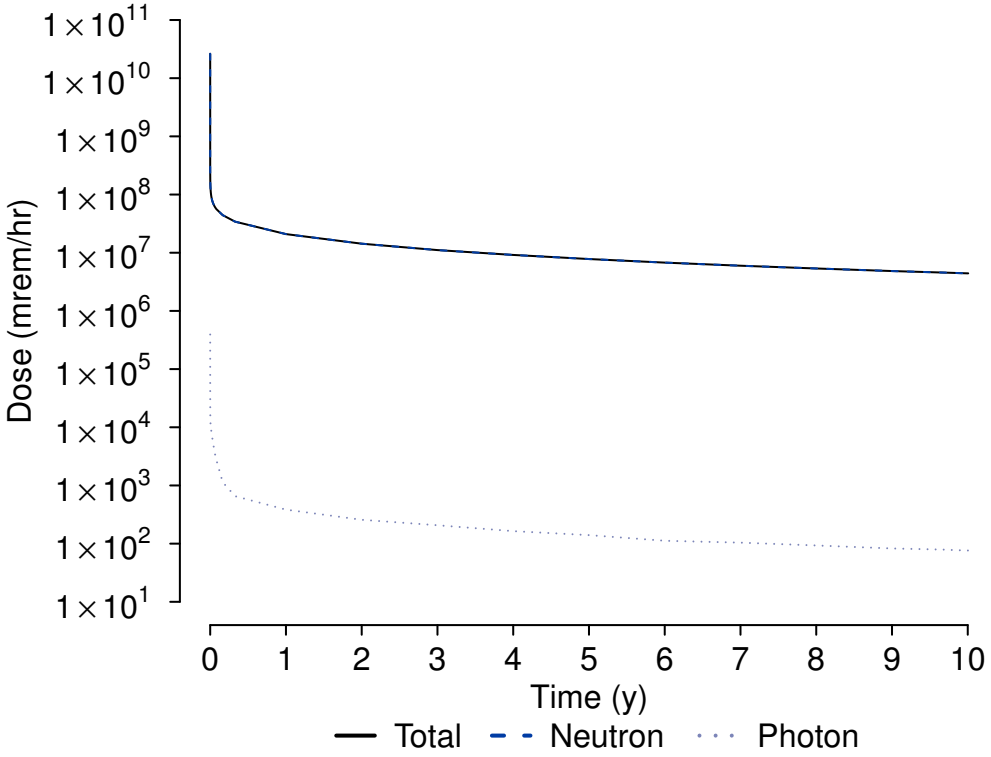

Figure 5.17: Predicted dose for the MSNB shielded by a proposed cask design following operation

radiation levels in proximity to a package during transport [27]:

- 200 mrem/hr on the external surface of the package, unless the following conditions are met, in which case the limit is 1000 mrem/hr:
  - The shipment is made in a closed transport vehicle;
  - The package is secured within the vehicle so that its position remains fixed during transportation; and
  - There are no loading or unloading operations between the beginning and end of the transportation;
- 200 mrem/hr at any point on the outer surface of the vehicle, including the top and underside of the vehicle; and
- 10 mrem/hr at any point 2 meters from the outer lateral surfaces of the vehicle; and
- 2 mrem/hr in any normally occupied space

With the assumption that the conditions outlined in the regulation of the surface dose rate are met, the equivalent dose produced by the unshielded MSNB at the conclusion of a 10 year cooldown period must be reduced to 1000 mrem/hr, or 0.002% of the predicted dose. The proposed cask design, which reduces the dose after the 10 year period to $4.42 \cdot 10^6$ mrem/hr, must further reduce the dose to 0.023% to be acceptable for transport.

Chapter 6: Summary and Conclusions

6.1 Limitations and Assumptions

One of the most significant assumptions used throughout this investigation was that of the density of the FLiBe-UF_4 eutectic. The density of the mixture influenced every assessment of the MSNB performance because of its use in calculating the mass of ^{235}U in the system and the spacing between adjacent atoms of the fissile fuel. Varying the density used in the MCNP and ORIGEN models would result in suboptimal control rod performance, new rates of production of fission products, and potentially the inability to bring the system into a subcritical configuration. The combination of the uncertainty of the density and the inclusion of only a few neutron data libraries with evaluation temperatures near the temperatures expected in the MSNB also limited the ability of MCNP to fully simulate thermal effects on the system neutronics.

In the determination of the radioactive dose experienced in proximity to the MSNB following its operational period, the source used for evaluating the flux of radiation escaping the reactor was assumed to be only the eutectic-containing cells in the MCNP model. In reality, all of the components of the reactor would have been irradiated during operation and contribute to the radiation escaping the system.

Simulation of the MSNB only as a static, rather than dynamic, system with MCNP was one of the most significant limitations of the system. There were some physical characteristics and effects noted in the system that MCNP is not suited to reproduce, such as the vortices along the edges of the MSNB core, the perpetual homogenization of the UF_4 in the FLiBe as it was depleted within the critical core, and production and buildup of ^{135}Xe in the system during operation. However, there is a precedent for using MCNP to model liquid fuel systems. In a neutronic study conducted by Brovchenko et al., the performance of a conceptual molten salt fast reactor design was independently evaluated by a number of international teams [28]. Two of the seven participating institutions used MCNP or a variant of the code; one participant used MCNP "as is," while the other used MCNP4B coupled with ORIGEN. Other notable codes used by the other collaborators include: DYN3D-MSR, a coupled neutronics and thermal-hydraulics code specially developed for modeling MSRs [29]; Serpent-2, a multi-physics code that couples Monte Carlo particle transport with thermal-hydraulics and CFD [30]; and DALTON, coupled with LOWFAT, which simultaneously solves the neutron diffusion and modified Bateman equations [31]. Brovchenko et al. observed that "only small discrepancies were thereby observed for the evaluations based on different computational tools ... while the choice of the nuclear database has a more consequent impact on all the results."

As a result of the limitations of MCNP, several assumptions were made in simulating the operation of the MSNB. Most significantly, it was assumed that ^{135}Xe would build to an equilibrium determined by the neutron flux of the system rather than the saturation point of the gas in the eutectic. At each timestep of the simulation, the concentration of the radionuclide was reset to a fixed value or removed entirely, or the buildup of the neutron poison was not tracked at all.

6.2 Future Work

Future work on the subject of the MSNB neutronics should focus first on addressing the assumptions and limitations addressed in Section 6.1. Most importantly, efforts should be made to address the assumption of the density of the FLiBe-UF_4 eutectic. The density of the mixture should be experimentally verified throughout the range of UF_4 compositions and temperatures expected in the MSNB system.

Computational tools that couple thermal-hydraulics and neutronics simulations should be used to verify and validate the results produced in this study. A promising candidate code for this task is Serpent-2. Codes that are able to couple these simulations to calculations of chemical and molecular properties would enable more complete simulations of the processes involved in the operation of the MSNB, fully replicating the effects of fluid flow, fission product production, and fissile fuel burnup in the reactor.

Finally, more complete burnup and fission product simulations should be conducted that simulate the effects of the neutron flux on other reactor materials, including the BeO reflector and stainless steel structural components. The buildup of fission products in these materials may affect the criticality of the system, and will affect the radioactive dose in proximity to the reactor.

6.3 Conclusion

The MSNB is capable of producing 10 MW of thermal power and operating between 6 and 10 years, or more, without requiring refueling or reprocessing of the FLiBe-UF_4 eutectic. To achieve these operational requirements, the MSNB utilizes ^{235}U enriched to 20% and dissolved in the FLiBe molten salt as UF_4, which constitutes 7% of the mass of the eutectic mixture. The rotating control rod design optimized for use in this configuration allows for control of the fission chain reaction, maintains a uniform neutron flux profile across the radial and axial profiles of the reactor core, and is capable of placing the reactor in a subcritical configuration at the beginning of operation. The safety of the system is enhanced by thermal effects that produce a large negative reactivity coefficient with increasing coolant temperatures. Fission products built up in the system during operation, and the radiation emitted by these radionuclides following operation, were calculated and used to inform the design of a transportation cask. These analyses demonstrate that the MSNB is a promising candidate to meet the need for a reliable source of small-scale electrical power.

References

[1] Roadmap for the Deployment of Micro-Reactors for U.S. Department of Defense Domestic Installations. NEI Technical Report, Nuclear Energy Institute, October 2018.

[2] Jérôme Serp, Michel Allibert, Ondřej Beneš, Sylvie Delpech, Olga Feynberg, Véronique Ghetta, Daniel Heuer, David Holcomb, Victor Ignatiev, Jan Leen Kloosterman, Lelio Luzzi, Elsa Merle-Lucotte, Jan Uhlíř, Ritsuo Yoshioka, and Dai Zhimin. The molten salt reactor (MSR) in generation IV: Overview and perspectives. *Progress in Nuclear Energy*, 77:308–319, November 2014.

[3] US Department of Energy Nuclear Energy Research Advisory Committee. Molten Salt Reactor, December 2002.

[4] Manohar S. Sohal, Matthias A. Ebner, Piyush Sabharwall, and Phil Sharpe. Engineering Database of Liquid Salt Thermophysical and Thermochemical Properties. Technical Report INL/EXT-10-18297, Idaho National Laboratory, March 2010.

[5] D.T. Ingersoll, C.W. Forsberg, and P.E. MacDonald. Trade Studies on the Liquid-Salt-Cooled Very High-Temperature Reactor: Fiscal Year 2006 Progress Report. Technical Report ORNL/TM-2006/140, Oak Ridge National Laboratory, Oak Ridge, Tennessee, February 2007.

[6] Roberto Serrano-López, Jordi Fradera, and Santiago Cuesta-López. Molten salts database for energy applications. *Chemical Engineering and Processing: Process Intensification*, 73:87–102, November 2013. arXiv: 1307.7343.

[7] Richard M. Felder and Ronald W. Rousseau. *Elementary Principles of Chemical Processes*. Wiley, Hoboken, NJ, 3 edition, December 2004.

[8] Sukhvinder P.S. Badwal, Sarbjit Giddey, and Christopher Munnings. Hydrogen production via solid electrolytic routes. *Wiley Interdisciplinary Reviews: Energy and Environment*, 2(5):473–487, September 2012.

[9] Nuclear Costs in Context. Technical report, Nuclear Energy Institute, Washington, DC, October 2018.

[10] Glenn F. Knoll. *Radiation Detection and Measurement*. Wiley, Hoboken, N.J, 4 edition, August 2010.

[11] Iván Lux and László Koblinger. *Monte Carlo Particle Transport Methods: Neutron and Photon Calculations*. CRC Press, March 1991.

[12] Forrest B. Brown. Monte Carlo Techniques for Nuclear Systems - Theory Lectures, 2016.

[13] MCNP User's Manual Code Version 6.2. Technical Report LA-UR-17-29981, Los Alamos National Laboratory, Los Alamos, NM, October 2017.

[14] V. V. Ignat'ev, A. V. Merzlyakov, V. G. Subbotin, A. V. Panov, and Yu. V. Golovatov. Experimental investigation of the physical properties of salt melts containing sodium and lithium fluorides and beryllium difluoride. *Atomic Energy*, 101(5):822–829, November 2006.

[15] John R. Lamarsh and Anthony J. Baratta. *Introduction to Nuclear Engineering*. Pearson, Hoboken, NJ, 4 edition, January 2017.

[16] R.J. McConn, C.J. Gesh, R.T. Pagh, R.A. Rucker, and R.G. Williams. Compendium of Material Composition Data for Radiation Transport Modeling. Technical Report PNNL-15870, Pacific Northwest National Laboratory, Richland, WA, March 2011.

[17] The JEFF-3.0 Nuclear Data Library. Technical Report NEA No. 3711, Nuclear Energy Agency, 2005.

[18] W. Wieselquist. SCALE Code System - ORIGEN: Neutron Activation, Actinide Transmutation, Fission Product Generation, and Radiation Source Term Calculation. Technical Report ORNL/TM-2005/39, Oak Ridge National Laboratory, March 2018.

[19] Gašper Žerovnik, Manca Podvratnik, and Luka Snoj. On normalization of fluxes and reaction rates in MCNP criticality calculations. *Annals of Nuclear Energy*, 63:126–128, January 2014.

[20] Said Mughabghab. *Atlas of Neutron Resonances - Resonance Parameters and Thermal Cross Sections Z=1-100*. Elsevier Science, 5 edition, March 2006.

[21] Balraj Singh, Alexander A. Rodionov, and Yuri L. Khazov. Nuclear Data Sheets for A = 135. *Nuclear Data Sheets*, 109(3):517–698, March 2008.

[22] U.S. Department of Energy. *DOE Fundamentals Handbook - Nuclear Physics and Reactor Theory*, volume 2. U.S. Department of Energy, Washington, DC, 1 edition, January 1993.

[23] J.E. Purcell and C.G. Sheu. Nuclear Data Sheets for A = 3. *Nuclear Data Sheets*, 130:1–20, December 2015.

[24] Neil E. Todreas and Mujid S. Kazimi. *Nuclear Systems Volume I: Thermal Hydraulic Fundamentals*. CRC Press, Boca Raton, FL, 2 edition, September 2011.

[25] Data for Protection against Ionizing Radiation from External Sources: Supplement to ICRP Publication 15. Technical Report ICRP Publication 21, International Commission on Radiological Protection, 1973.

[26] United States Nuclear Regulatory Commission. 10 C.F.R. § 20.1004, 2019.

[27] United States Nuclear Regulatory Commission. 10 C.F.R. § 71.47, 2019.

[28] A. Buerkholz. Irradiation Damage in Beryllium Oxide. Technical Report EUR-3054.e, Centre d'Etude de l'Energie Nucleaire, Mol, Belgium, July 1966.

[29] Jiří Křepel, Ulrich Rohde, Ulrich Grundmann, and Frank-Peter Weiss. DYN3d-MSR spatial dynamics code for molten salt reactors. *Annals of Nuclear Energy*, 34(6):449–462, June 2007.

[30] Jaakko Leppänen. Serpent – a Continuous-energy Monte Carlo Reactor Physics Burnup Calculation Code. Technical report, VTT Technical Research Centre of Finland, June 2015.

[31] I. Lantzos. Molten Salt Fast Reactor: Shift from Burner to Breeder. Master's thesis, Delft University of Technology, March 2016.

Appendix A: Dose Conversion Factors

Energy (MeV)	**Conversion Factor** $\left(\frac{\mathbf{cm^{-2}\ s^{-1}}}{\mathbf{mrem\ hr^{-1}}}\right)$
$1.0 \cdot 10^{-2}$	360
$1.5 \cdot 10^{-2}$	900
$2.0 \cdot 10^{-2}$	1700
$3.0 \cdot 10^{-2}$	3900
$4.0 \cdot 10^{-2}$	6400
$5.0 \cdot 10^{-2}$	8300
$6.0 \cdot 10^{-2}$	9000
$8.0 \cdot 10^{-2}$	8300
$1.0 \cdot 10^{-1}$	6800
$1.5 \cdot 10^{-1}$	4200
$2.0 \cdot 10^{-1}$	2900
$3.0 \cdot 10^{-1}$	1800
$4.0 \cdot 10^{-1}$	1300
$5.0 \cdot 10^{-1}$	1100
$6.0 \cdot 10^{-1}$	8800
$8.0 \cdot 10^{-1}$	6800
$1.0 \cdot 10^{0}$	5600
$1.5 \cdot 10^{0}$	4100
$2.0 \cdot 10^{0}$	3300
$3.0 \cdot 10^{0}$	2500
$4.0 \cdot 10^{0}$	2100
$5.0 \cdot 10^{0}$	1800
$6.0 \cdot 10^{0}$	1600
$8.0 \cdot 10^{0}$	1300
$1.0 \cdot 10^{1}$	1100
$2.0 \cdot 10^{1}$	6400

Table A.1: Energy-dependent flux-to-dose conversion factors for photons

Energy (MeV)	**Quality Factor**	**Conversion Factor** $\left(\frac{\mathbf{cm^{-2}\ s^{-1}}}{\mathbf{mrem\ hr^{-1}}}\right)$
$2.5 \cdot 10^{-8}$	2.0	272.2
$1.0 \cdot 10^{-7}$	2.0	272.2
$1.0 \cdot 10^{-6}$	2.0	225.0
$1.0 \cdot 10^{-5}$	2.0	225.0
$1.0 \cdot 10^{-4}$	2.0	233.3
$1.0 \cdot 10^{-3}$	2.0	272.2
$1.0 \cdot 10^{-2}$	2.5	280.6
$1.0 \cdot 10^{-1}$	7.5	47.2
$5.0 \cdot 10^{-1}$	11.0	10.8
$1.0 \cdot 10^{0}$	11.0	7.5
$2.5 \cdot 10^{0}$	9.0	8.1
$5.0 \cdot 10^{0}$	8.0	6.4
$7.0 \cdot 10^{0}$	7.0	6.7
$1.0 \cdot 10^{1}$	6.5	6.7
$1.4 \cdot 10^{1}$	7.5	4.7
$2.0 \cdot 10^{1}$	8.0	4.4

Table A.2: Energy-dependent radiation quality and flux-to-dose conversion factors for neutrons